Alma Mater Studiorum Università degli Studi di Bologna

SCUOLA DI SCIENZE
Dipartimento di Fisica ed Astronomia
Corso di Laurea Magistrale in Astrofisica e Cosmologia

Radiative Transfer Modeling for AGN feedback

Tesi di Laurea Magistrale

Candidato:
Cristiano Fanelli

Relatore:
Chiar.mo Prof. **Luca Ciotti**

Co-relatori:
Chiar.ma Prof.ssa **Silvia Pellegrini**
Dott. **Andrea Negri**

Sessione III
Anno accademico 2016/2017

ὅταν βλέπω σε, προσκυνῶ, καὶ τους λόγους.
τῆς παρθένου τὸν οἶκον ἀστρῷον βλέπων
εἰς οὐρανὸν γάρ ἐστι σοῦ τὰ πράγματα,
Ὑπατία σεμνή, τῶν λόγων εὐμορφία,
ἄχραντον ἄστρον τῆς σοφῆς παιδεύσεως.

Quando ti vedo mi prostro davanti a te e alle tue parole,
vedendo la casa astrale della Vergine,
infatti verso il cielo è rivolto ogni tuo atto
Ipazia sacra, bellezza delle parole,
astro incontaminato della sapiente cultura.
***Pallada d'Alessandria**, IV sec. d.C.*

Abstract

Nowadays, there is agreement in the scientific community that active galaxies are actually normal galaxies that they experience periodically a phase of nuclear activity, due to gas accretion on central massive black hole. As a consequence, AGN feedback study has increased in recent years with the aim of shedding light on its role in the galaxy evolution framework.

From a theoretical perspective, many works have been made on this phenomenon, in particular hydrodynamical simulations, which try to "catch" AGN feedback as a physical process and its impact on galaxy evolution. There are two types of feedback from AGN, one is the *mechanical* feedback, and the other is the *radiative* feedback. Because of the difficulty to simulate the radiative AGN feedback phenomenon, both for its intrinsic complexity and the arduous task of its implementation in hydro codes, many works take into account just the mechanical AGN feedback.

The aim of this work is to realize a new modeling of radiative transfer consistent with the AGN feedback process in elliptical galaxies. We have studied this model accurately from an analytical perspective, and we have shown its main properties; after that we have tested it in post-processing, using temperature and density maps from high resolution hydrodynamical simulations, in which we have considered the absorption of the medium due to photoionization and dust. Dust is important because it absorbs radiation differently with the change of wavelength. Finally, we have compared our model with another present in the literature.

We have found that this new radiative transport model can be used both to directly treat the AGN feedback problem, and also as a benchmark for other algorithms, which are faster from a numerical point of view, and that aim to treat the AGN feedback problem.

Sommario

Un'idea oggi accettata dalla comunità scientifica, è che le galassie attive siano delle galassie "normali" che periodicamente, per un periodo limitato, entrano in una fase di attività nucleare (AGN), dovuta all'accrescimento di gas da parte del loro buco nero massiccio centrale. Di conseguenza, lo studio del fenomeno di AGN feedback si è intensificato molto in questi ultimi anni, con l'obiettivo di fare chiarezza sul ruolo dell'AGN feedback nell'evoluzione delle galassie.

Dal punto di vista teorico sono stati fatti molti lavori a proposito, in particolare simulazioni idrodinamiche, in quanto cercano di "catturare" il fenomeno fisico di AGN feedback e anche l'impatto che questo ha sull'evoluzione globale delle galassie.Esistono due tipi di feedback, quello *meccanico* e quello *radiativo*. Data la difficoltà di simulare l'AGN feedback radiativo a causa della complessità del fenomeno fisico in se e dell'implementazione numerica in codici idrodinamici, nella maggior parte dei lavori si è tenuto conto principalmente del Feedback meccanico da AGN.

Lo scopo di questo lavoro è stato quello di trovare un nuovo modellamento del trasporto radiativo consistente con il fenomeno di AGN feedback in galassie ellittiche. Abbiamo studiato questo modello rigorosamente da un punto di vista analitico delineandone le caratteristiche principali, dopodichè lo abbiamo testato in post-processing su mappe di temperatura e densità, output di simulazioni idrodinamiche ad alta risoluzione, tenendo conto dell'assorbimento dovuto a processi di ionizzazione e da parte della polvere. La polvere è importante perchè assorbe la radiazione in maniera differente al variare della lunghezza d'onda. Lo abbiamo infine confrontato con un altro modello presente in letteratura, creato anch'esso per essere applicato al problema di AGN feedback radiativo.

Abbiamo trovato che questo nuovo modellamento di trasporto radiativo può essere utilizzato sia per trattare direttamente il problema di AGN feedback in maniera consistente, sia come banco di prova di altri algoritmi, più veloci da un punto di vista numerico, che si prefiggono di trattare lo stesso problema.

Contents

1 Introduction **1**
- 1.1 Observational Evidence of AGN feedback . . . 2
- 1.2 Purpose of the Thesis . . . 11

2 Radiative Transfer Modeling **15**
- 2.1 Basics on Radiative Transfer . . . 15
- 2.2 The Radiative Transfer equations . . . 19
- 2.3 The D Model . . . 24
- 2.4 The AD Model . . . 26
- 2.5 Closed Form of the AD Equations . . . 29
  - 2.5.1 Integration of the D Equation . . . 30
  - 2.5.2 Integration of the A Equation . . . 33
- 2.6 Discussion . . . 36

3 The Interstellar Medium of Early-type Galaxies **39**
- 3.1 Passive Stellar evolution: Mass Losses & Heating . . . 40
- 3.2 Gas Physics . . . 43
  - 3.2.1 Compton Heating . . . 46
  - 3.2.2 Partially Ionized Gas Clouds . . . 48
  - 3.2.3 Electron Scattering . . . 50
- 3.3 Dust Physics . . . 51

4 Post Processing Study of AGN Radiative Feedback: Main Results **55**
- 4.1 Study Case . . . 56
- 4.2 D Model . . . 60
  - 4.2.1 Photoionization Physics . . . 60
  - 4.2.2 Photoionization and Dust Physics . . . 61
- 4.3 AD Model . . . 65
  - 4.3.1 Photoionization Physics . . . 65
  - 4.3.2 Photoionization and Dust Physics . . . 67

4.4 AD Model vs. N12 Model 71

5 Discussions and Conclusions **79**
5.1 Future Prospects 81

A Geometry of Radiative Transfer equation **83**

Bibliography **87**

Chapter 1

Introduction

Until recently, astronomers thought that normal galaxies and quasars were two different astrophysical objects. It has been realized over the past decades that the central MBH (Massive Black Hole) that habits the center of most galaxies, is not just a peddling ornament of the host galaxy, but it is the link between normal galaxies and quasars. Furthermore, it seems that the central MBH may play a leading role in galaxy evolution, and it appears that it has a role also in determining the main observational properties.

The process by which this occurs is known as AGN (active galactic nuclei) feedback, and it takes place through an interaction between the energy and radiation generated by accretion onto the massive black hole and the gas in the host galaxy.

In this introduction we are going to present briefly the role of AGN feedback as it appears from observations and numerical simulations; then we will focus on the importance of the Radiative Feedback of AGN (and the difficulty of modeling it). Finally, we will show the outline of this work.

1.1 Observational Evidence of AGN feedback

Many elliptical galaxies contain central MBHs, and also contain substantial amounts of hot gas ($10^6 - 10^7$ K) capable of accreting onto the central MBH as a result of having cooling times that are short compared to the Hubble time. These MBHs have an intriguing relationship with the host galaxies, which is witnessed by observations and theoretical works. One of the most important of these relations is the *Magorrian Relation* (Magorrian et al. 1998), that links the mass of the central MBH with the mass of the stellar spheroid in which it lives (Fig. 1.1). When we say "stellar spheroid" we mean

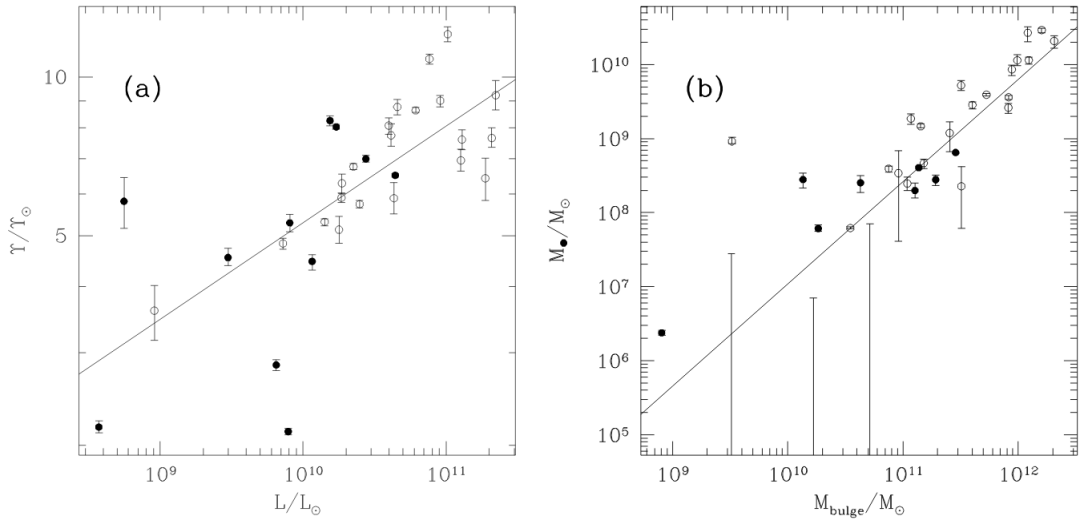

Figure 1.1: Correlations (a) between V-band stellar mass-to-light ratio Υ and bulge luminosity L and (b) between MDO (Massive Dark Object) mass M_{BH} and M_{bulge}. The filled and open circles plot power-law and core galaxies, respectively. The error bars give the 68% confidence intervals on Υ and M_{BH} (from Magorrian et al. 1998).

the bulge, if we are talking about disc galaxies, or the whole mass stellar content of early-type galaxies.

This scenario has been confirmed with the discovery of a new scaling law of MBH and their host galaxies, because of the increase of telescopes accuracy and the large amount of new data: the popular $M - \sigma$ relation. This law was independently discovered and announced at the Spring 2000 meeting of the American Astronomical Society by Gebhardt (see Gebhardt, Bender, et al. 2000) and by Ferrarese, and published by Ferrarese (Ferrarese and Merritt 2000) and by Gebhardt (Gebhardt, Richstone, et al. 2000). Thus, in the latter two decades astronomers were convinced by observations (Fabian 2012) that in every normal galaxies resides a MBH, and this may be the link between AGN and normal galaxies. So, the typical morphology of today galaxies, such as the "dead and boring red objects" known as elliptical galaxies (from Ciotti 2009) can be produced by episodic AGN bursts. However, we have to understand if the central MBH can affect the evolution of the host galaxy.

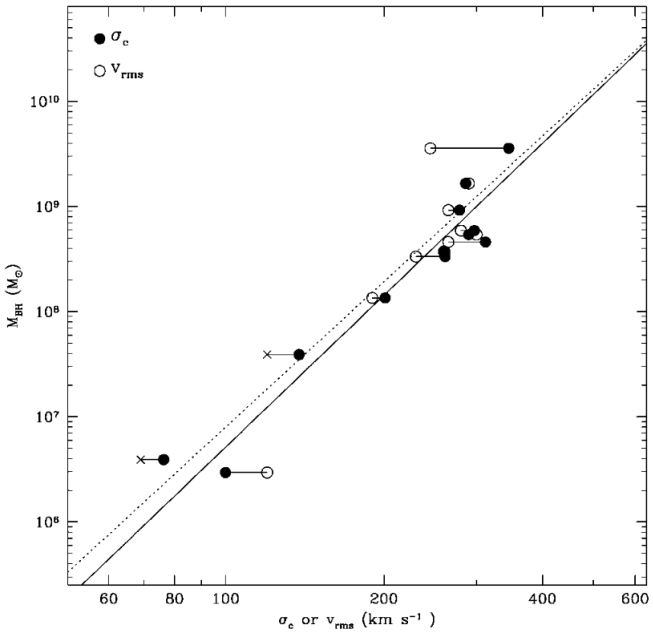

Figure 1.2: BH mass vs the central velocity dispersion σ_c of the host elliptical galaxy or bulge (filled circles) or the rms velocity v_{rms} measured at one-fourth of the effective radius (open circles). Crosses represent lower limits in v_{rms}. The solid and dashed lines are the best linear fits using σ_c and v_{rms}, respectively (Ferrarese and Merritt 2000).

The volume occupied by the central MBH is $\sim 10^{27}$ smaller than the whole galaxy, so can the MBH drive the evolution and modify the environment in which it lives, the host galaxy?

It is quite easy to demonstrate that the growth of the central MBH by accretion can have a profound effect on its host galaxy. To answer this question, we can compare the binding energy of the galaxy:

$$E_{gal} \approx M_\star \sigma^2 \tag{1.1}$$

with the energy released by the growth of the black hole:

$$E_{BH} \approx \epsilon M_{BH} c^2 \ , \tag{1.2}$$

where $M_\star$ is the stellar mass of the galaxy, σ is the central velocity dispersion of the stars, ϵ is the radiative electromagnetic efficiency, M_{BH} is the MBH mass and c is the speed o light.

From Fig. 1.1 we can see that $M_{BH} \approx 1.4 \cdot 10^{-3} M_\star$ (Kormendy and Ho 2013), assuming a radiative electromagnetic efficiency for the accretion process of 10% ($\epsilon = 0.1$),

then the ratio between these energies is:

$$\frac{E_{BH}}{E_{gal}} = \frac{\epsilon \cdot 1.4 \cdot 10^{-3} M_\star c^2}{M_\star \sigma^2} \tag{1.3}$$

that becomes:

$$\frac{E_{BH}}{E_{gal}} \approx 1.4 \cdot 10^{-4} \left(\frac{c}{\sigma}\right)^2 , \tag{1.4}$$

that says us how much the energy associated with the MBH is important compared to the binding energy of the galaxy.
Most galaxies have $\sigma < 400 km/s$, so we obtain that $\frac{E_{BH}}{E_{gal}} > 80$: the energy produced by the growth of the black hole exceeds the binding energy by a large factor. If even a small fraction of the energy can be transferred to the gas, then an AGN can have a profound effect on the evolution of its host galaxy.

There are principally two regimes in which the MBH accretes mass from around itself, that are called *radiative mode* (knowing also as *quasar*) and *kinetic mode* (also known as the *radio jet*, or *maintenance mode.*), which are quite different from each other. The radiative mode operates in a typical bulge when the accreting black hole luminosity is close to the Eddington limit, which is given by:

$$L_{Edd} = \frac{4\pi G M_{BH} m_p c}{\sigma_T} . \tag{1.5}$$

The 1.5 refers to a pure ionized hydrogen gas, where G is the gravitational constant, M_{BH} is the MBH mass, m_p is the proton mass and σ_T is the Thomson cross-section, defined by the Thomson scattering. If we substitute the constant quantities in the 1.5, then we obtain:

$$L_{Edd} \simeq 3.2 \cdot 10^4 \left(\frac{M_{BH}}{M_\odot}\right) L_\odot = 1.26 \cdot 10^{38} \left(\frac{M_{BH}}{M_\odot}\right) erg/s , \tag{1.6}$$

and this says us that to have a luminosity of the order of quasar luminosity $\sim 10^{46} erg/s$, we must have a MBH with a mass of at least $\sim 10^8 M_\odot$, which is consistent with the MBHs that reside at the center of galaxies (Fig. 1.1 , Fig. 1.2).

The massive galaxies at the centre of groups and clusters are often surrounded by gas with a radiative cooling time short enough that a cooling flow should be taking place (Fabian 1994). We have that in the central region of galaxy clusters there is a huge amount of radiation in the X-rays, which indicates a large radiative loss and mass cooling rates of tens, hundreds or even thousands of $M_\odot yr^{-1}$:

$$\dot{M} = \frac{2}{5} \frac{L \mu m}{kT} \tag{1.7}$$

where μm is the mean mass per particle of the gas with temperature T, and L is the luminosity (mostly emitted in the X-ray band). These short cooling times, due to high gas density (the cooling goes as $\sim \rho^2$, where ρ is the density), in these massive galaxies sometimes are good to establish an accretion of gas with a low value of L/L_{Edd}, thus, a kinetic mode, in which we can have also the formation of radio jets; this is the way kinetic accretion works.
Another phenomenon that provides a large amount of gas falling onto the central MBH is merging. Interactions and mergers can strongly affect galaxy evolution. Since the early studies by A. Toomre and J. Toomre (1972), it is generally believed that interactions can trigger starburst processes in galaxies, via tidal effects. The fact that interacting galaxies are more luminous in the far infrared (FIR) (e.g. Sanders and Mirabel 1996) and in the radio band (e.g. Hummel 1981), and that they have larger H_α equivalent widths (e.g. Kennicutt et al. 1987) supports this hypothesis. The star formation (SF) is found to be stronger in the nucleus, although it is also enhanced in the disc. A widely accepted idea, supported by simulations, is that galaxy interactions induce flows of gas from the outer parts of the galaxy and/or the companion into the inner regions through loss of the angular momentum induced by tidal forces and then, trigger nuclear activity. Furthermore, many astronomer have found that quasar host galaxies show distorted morphologies, reminiscent of past merging events (e.g. Bahcall et al. 1997). In Fig. 1.3 we can see some example.
Nevertheless, other found no evidence of past interactions (e.g.Dunlop et al. 2003) in QSOs, so probably merging is not the only phenomenon that can trigger accretion onto MBH.

However, it is not clear if the fraction of AGN host galaxies undergoing interactions is really larger than the fraction of inactive galaxies undergoing interactions, but we can say that merging is a physics process that may provide gas accretion in the central region of galaxies, and then trigger nuclear activity.

Other physical processes that can pile up gas in the central region of galaxies are the so-called "secular processes", that can have both external and internal origin. With external origin we mean a slow and continuous external matter accretion, with typical structures such as streams or halos (known also as hot and cold mode accretion). For isolated AGN we have that the only source of gas is the mass loss from evolving stars. So also for isolated galaxies, we know that the recycled gas from dying stars is an important source of fuel for the central MBH, even in absence of external phenomena such as galaxy merging, that are often advocated as the way to induce QSO activity (Ciotti and Ostriker 1997, Ciotti and Ostriker 2001, Ciotti and Ostriker 2007, Ostriker et al. 2010, Ciotti, Ostriker, and Proga 2010, Ciotti, Pellegrini, et al. 2017).

In Fig. 1.4 we have a summary of various accretion modes and the conditions in which these may take place.
There are a lot of observational evidence of the importance of AGN feedback in massive galaxies, groups and clusters. At large scale ($\sim 1Mpc$) powerful jets can trigger the evolution of the hot ICM (Intra Cluster Medium), modifying its content of gas and its metal distribution, because of it can have a positive feedback on ISM of host galaxy and

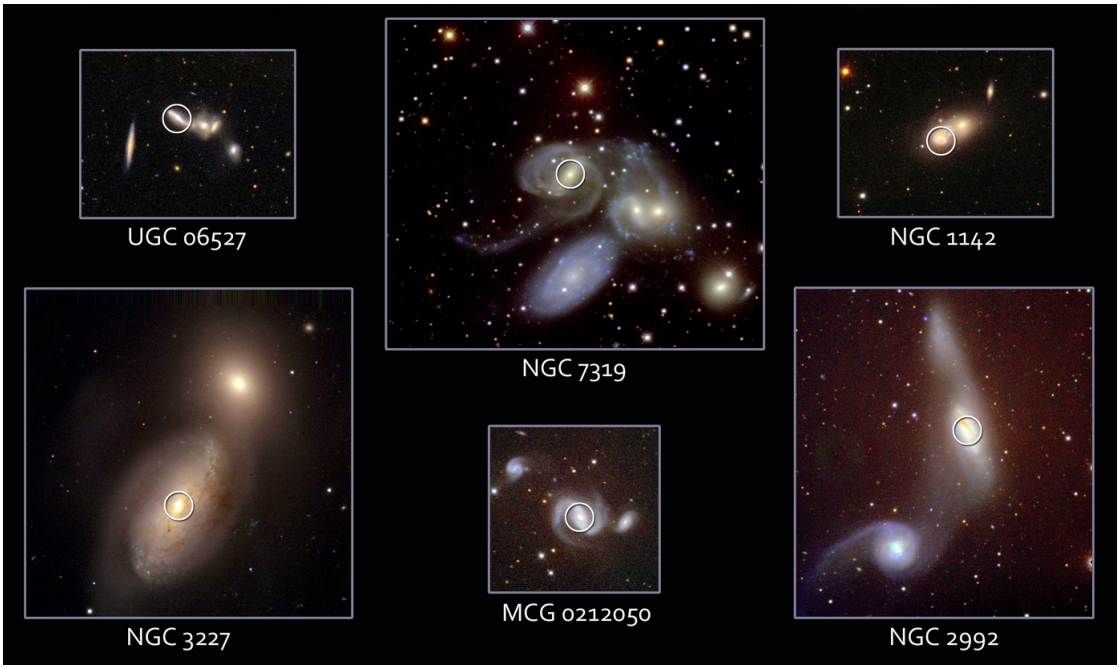

Figure 1.3: These images show the optical counterparts of several AGN detected by the Swift BAT Hard X-ray Survey. The galaxy shapes are either physically intertwined or distorted by the gravity of nearby neighbors. The active black holes (circled) were known prior to the Swift survey, but Swift has found dozens of new AGN in more distant galaxies.

start up star formation, which enriches the gas with metal via SNe (and eventually, they also expels the gas out of the galaxy and so in the ICM).Galaxy clusters and groups are a perfect laboratory to study also the past AGN events from the cD (central Dominant) galaxy for example, and also the feedback on the ICM.

As we can see in the Perseus Cluster in Fig. 1.5 from Fabian et al. (2006), there are a lot of "disturbances" on the ICM caused by AGN feedback from the central galaxy (NGC 1275): we can see *shock front*, *cavities* and probably the more interesting, smoking gun of past AGN activity, the so-called *ghost bubbles* (which vaguely remember the air bubbles of the divers when they go back to the surface of the water and become pancake-shaped). These are probably the best evidence of AGN feedback; the presence of these ghost bubbles and cavities can be a confirmation of the fact that AGN actually is an episodic phenomenon, and it switch on and off repeatedly over cosmic time.

Similar studies have been made for M87 Galaxy, in which we can see *shock fronts*, and also *cavities* produced by present AGN activity (Fig. 1.6).

In our work we will focus on accretion and feedback in elliptical galaxies generated by internal secular processes (primarily accretion of mass internally produced by stellar evolution, for example through red giant winds and planetary nebulae). In this case we have not taken in consideration the formation of jets, but we have taken in consideration

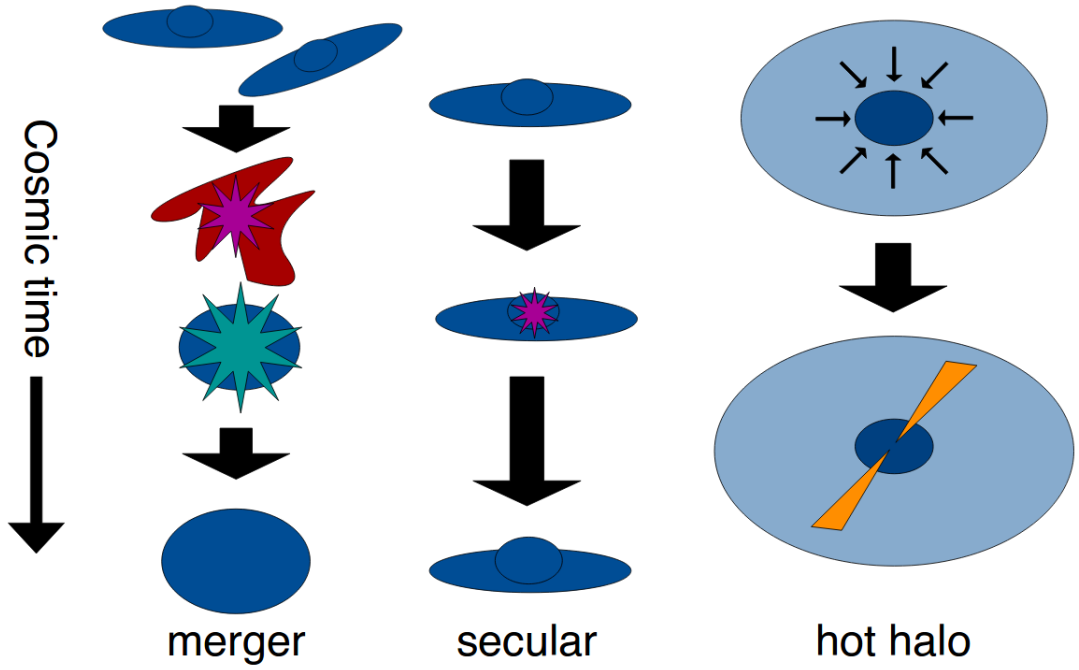

Figure 1.4: Schematic diagrams to illustrate the large-scale processes that are thought to be responsible for triggering AGN activity: major mergers of gas-rich galaxies, secular evolution (which includes both internal secular evolution and external secular evolution, the latter of which is driven by galaxy interactions), and hot halo accretion, which is presumed to be the dominatnt MBH growth mode for radio-loud AGNs (from Alexander and Hickox 2012).

the mechanical feedback due to the strong wind formed by the inflowing gas which is not consumed by SF or accreted on MBH. As gas is used up or blown away, a hot cavity is formed at the center of the system and, since a shock has propagated through that volume, it is essentially like a giant supernova remnant and one expects there to be particle acceleration and non-thermal radiation from the central region. Then, gradually this hot bubble cools and collapses and one returns to the normal elliptical, more or less in a quiescent phase. This wind comes from the Broad Line Region (BLR) of quasars: this is suggested by The outflow is evident in ultraviolet C_{iv} and Si_{iv} absorption lines with velocity shifts $v \sim 26,300\ km/s$ (Hamann et al. 2008). Generally, Broad Absorption Lines (BALs) in ultraviolet (UV) and X-Ray spectra of quasars are the main manifestation for such outflows, with velocities that can reach $\sim 0.2c$. Many observations show that AGN winds can be very complex flows, and neither spherical nor axial symmetry is applicable.

The structure, dynamics and evolution of a wind can be described by the equations of radiation magnetohydrodynamics. Possible wind driving mechanisms can be identified by three mechanisms: *Thermal Driving*, *Radiation Pressure Driving*, *Magnetic Driving*.

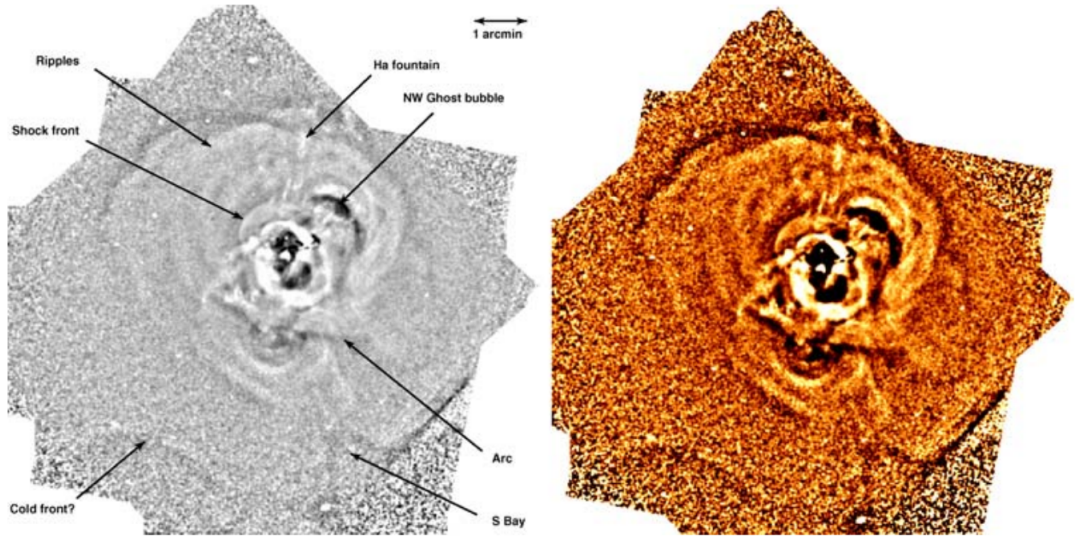

Figure 1.5: Unsharp mask image (with Chandra) made from the whole $0.3-7\ keV$ band by subtracting an image smoothed with a Gaussian of dispersion 10 arcsec from one smoothed by 1 arcsec and dividing by the sum of the two images. Various features are labelled in the lower contrast image at the left-hand side (from Fabian et al. 2006).

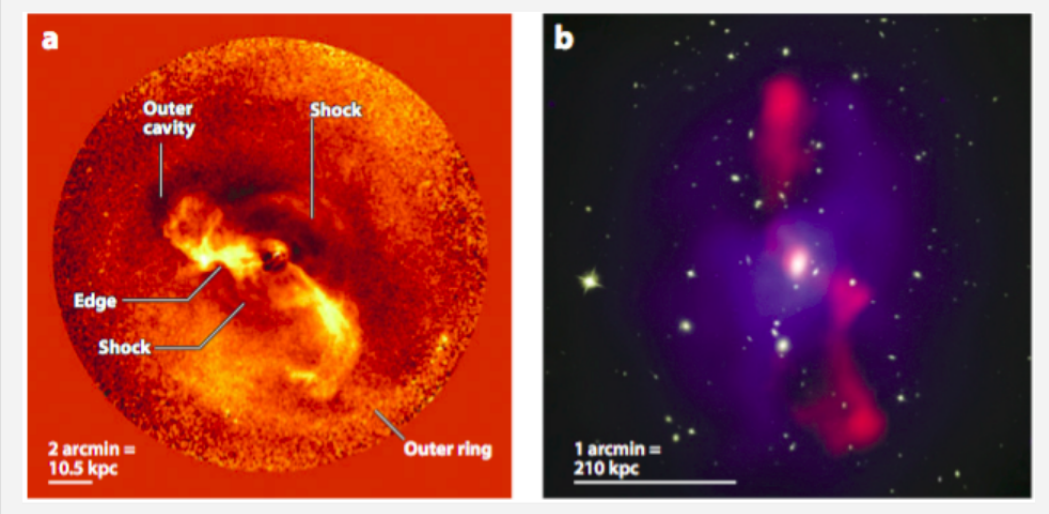

Figure 1.6: (a) M87 galaxy with its AGN jet shocking gas around it. (b) Radio lobes of the AGN (red) seen alongside x-ray ICM gas (blue), a clear signature of quantitative AGN feedback. From Fabian (2012).

Probably, as is often the case, it is not just one mechanism that drives the formation of these winds, but rather can be a combination of all these mechanisms, which can occur at different evolutionary stages of AGNs or in different places in the core of galaxies.

As first revealed by Einstein observations and deepened by Chandra and XMM-Newton, normal elliptical galaxies, both isolated or in groups and clusters, can show a significant emission in the $0.5-4.5\ keV$, ranging from 10^{39} to $10^{42}\ ergs^{-1}$. This emission is associated with hot gaseous halos within the galaxies, containing $M_{gas} \approx 10^{8}-10^{11} M_{\odot}$ (Fabbiano 1989). As shown by L. Ciotti and J.P. Ostriker in their series of papers, cooling flows and quasars can be different aspect of the same phenomenon (Ciotti and Ostriker 1997, Ciotti and Ostriker 2001, Ciotti and Ostriker 2007, Ostriker et al. 2010, Ciotti, Ostriker, and Proga 2010, Ciotti, Pellegrini, et al. 2017).
In this view, energy output (which can be either or both of radiative and mechanical) from the central MBH pushes matter out, the accretion rate drops precipitously and the expanding matter drives shocks into the galactic gas. As a consequence, the resulting hot bubble cools down via thermal processes (mainly bremsstrahlung cooling) and the consequent infall leads to renewed accretion and back to zero, the cycle repeats (Ciotti and Ostriker 2007). Moreover, AGN outbursts can trigger star formation (positive feedback) compressing cold dense clouds (which are near their Jeans or Bonnor-Ebert mass); this may pollute the early-type spectrum with the radiation of the new stars and as a consequence, we can see the *E+A spectrum* of some "normal" elliptical galaxies. In Fig.1.7 we can see a sum up of the elliptical galaxies - AGN life cycle, from Ciotti, Ostriker, and Proga (2010).

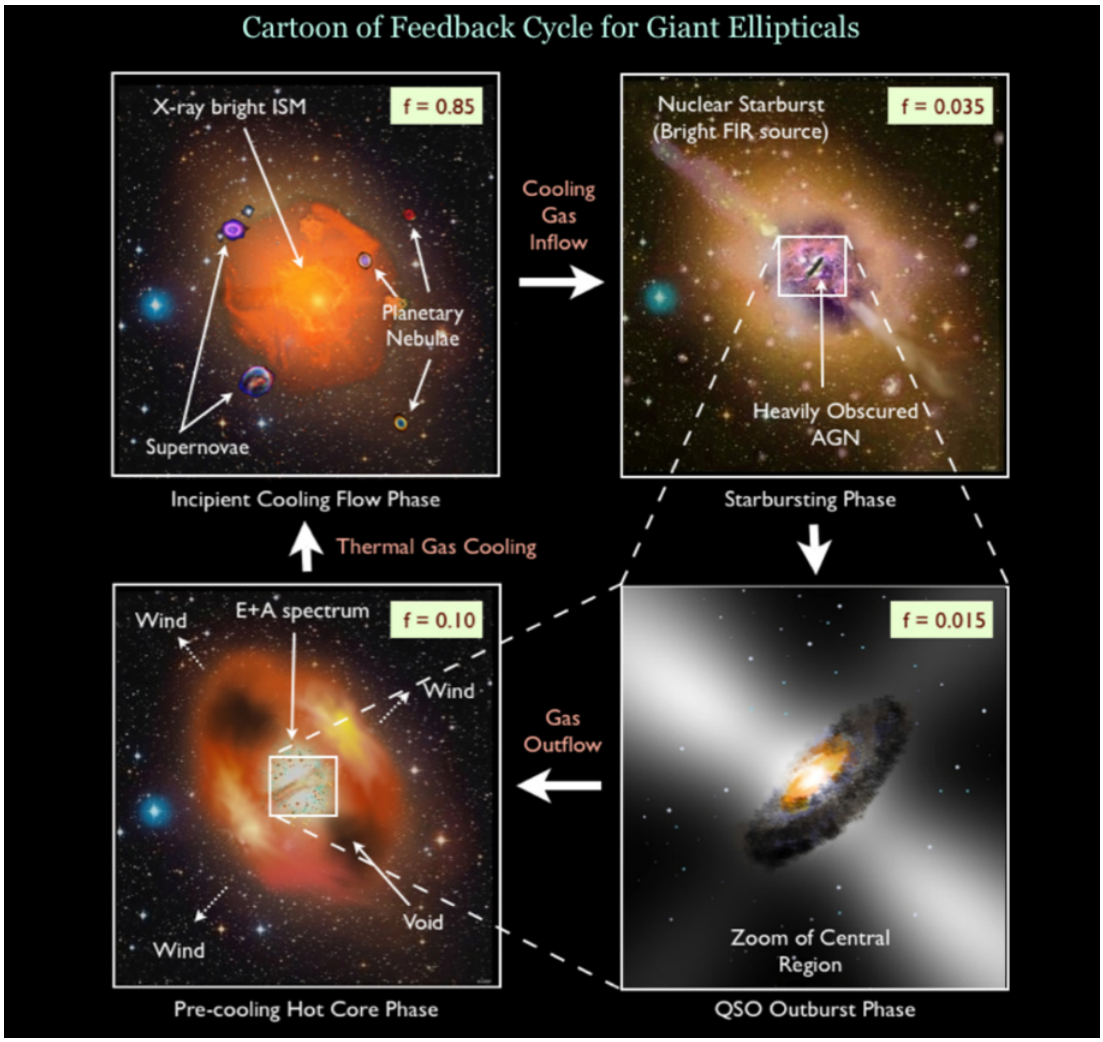

Figure 1.7: Four main phases of the feedback cycle in the life of a galaxy. Secondary gas from stellar evolution leads to a cooling-flow thermal instability that feeds a central MBH, the outbursts from which leads to an expanding hot bubble which terminates the inflow. The cycle may be repeated several times, and in each box there are the characteristic duty-cycle (f_{duty}) associated with each phase in a standard simulation. For detail see Ciotti, Ostriker, and Proga (2010).

1.2 Purpose of the Thesis

As we have seen in section 1.1, we do not need to invoke external processes, such as merging, in order to obtain quasar activity. In our study we take into account the evolution of an isolated elliptical galaxy,where its old stellar population evolving passively enriches the ISM with recycled gas (mass loss of red giants, planetary nebulae, SNe Ia). Cooling processes due to thermal instability of the hot halo (thermalized by the stellar motions and SNe Ia), cause the accretion on the central MBH which allows the galaxy to become an active galaxy.

These accretion events make the galactic nucleus very bright; it can reach $L \sim L_{Edd}\ erg/s$ and become a quasar. The luminosity of these astrophysical objects can reach $L \sim 10^{48}$ (the so-called high luminosity quasars), and this huge amount of radiation can have a great impact on the environment in which it lives.

As well known, radiation can interact with matter in very different ways. One of the biggest complication with the study of radiative transfer in astrophysical problems is to understand how the radiation interacts with the interstellar medium. The first complication is with the time scale of the system involving radiation and matter; the time scale variation of radiation is the speed of light c, whereas for the ISM we have that the time scale variation is the sound speed c_s which is, in the isothermal regime, given by:

$$c_s = \sqrt{\left(\frac{\partial P}{\partial \rho}\right)_T} = \sqrt{\frac{k_B T}{\mu m_p}} \tag{1.8}$$

whereas in the adiabatic regime the sound speed is:

$$c_s = \sqrt{\left(\frac{\partial P}{\partial \rho}\right)_S} = \sqrt{\gamma \frac{k_B T}{\mu m_p}} \tag{1.9}$$

where $\gamma = \frac{C_p}{C_v}$ and C_p is the specific heat at constant pressure, C_v is the specific heat at constant volume, k_B is the Boltzmann constant and T is the gas temperature.

For the typical range of temperature of the ISM, which ranges from 10 K to 10^7 K we have that the sound speed spreads from $\sim 3 \cdot 10^4\ cms^{-1}$ to $\sim 3 \cdot 10^7\ cms^{-1}$, with very little differences between the adiabatic and the isothermal cases. So we have that the ratio beteewn the time scales is $\frac{c}{c_s} \approx 10^3 - 10^6$, which is very high. From a numerical perspective, we can work just with the time scale computed with the speed of sound, because it is greather than that computed with the speed of light, but we have to be careful about it because, on the other hand, astrophysical distances are huge compared also with the speed of light: if we take a typical radius of elliptical galaxies $R_g \sim 100\ Kpc$, we have that a photon which starts from its centre takes a time of about $\frac{R_g}{c} \approx 10^5 yr$ to go through the whole galaxy, in a totally optically thin regime (in which photons react very little with the interstellar medium); as a consequence, on one hand we have that the light reacts quickly with the medium in whitch it propagates, but on the other hand

we have that from the moment the photon begins its path from the central region to the external one, the hydrodynamics changes.

From a numerical perspective, some approximations are needed, because we cannot work with an integration time-step computed with the speed of light: one choice for this approximation is to solve all of the radiative transfer equations assuming a steady state, therefore, the radiation field is considered to reach equilibrium instantaneously, and radiative forces are considered to act instantaneously in the whole galaxy. This is the approximation that we have also used in this work.

We want to study radiative transfer in a medium which can scatter, absorb and re-emit, and so we have other problems, in addition to the problem related to the time-step integration: we want to solve the radiation field on the whole integration domain, but we do not know the functional form of radiation field in advance; in addition, we have that the change of a "ray of light" in one position of the domain due to the characteristic of the medium (it can subtract, add or scatter photons), does not change just this ray, but has an impact on all the radiation field. Furthermore, if we want to be strict on treating radiative transfer, the interaction of the radiation field with matter has an impact directly on the medium, so it can changes density, coefficient absorption, and so on. In Fig. 1.8 we can see the complexity of the medium in which radiation propagates.

If we want to treat radiative transfer in dusty media, it gets more tricky: dust is one of the most important constituents of the interstellar medium (ISM). By mass it is only a small fraction: somewhere between 1% and 2%, but it has a great impact on the evolution of radiation field. From a chemical perspective dust grains are important because they have surfaces on which chemical reactions can take place much easier than in the gas phase. From a radiative transfer perspective they are important because they have strong continuum opacities. Furthermore, this opacity changes with the variation of the electromagnetic spectrum wavelength, and are thus much more capable of affecting radiative heat transfer than gas opacities. Moreover, dust extinction can “protect” certain regions of the interstellar medium from ultraviolet photons, thus enabling molecules to form in those regions. Finally, dust absorbs radiation in some wavelengths, and it re-emits this radiation at other wavelengths (not necessarily isotropically).

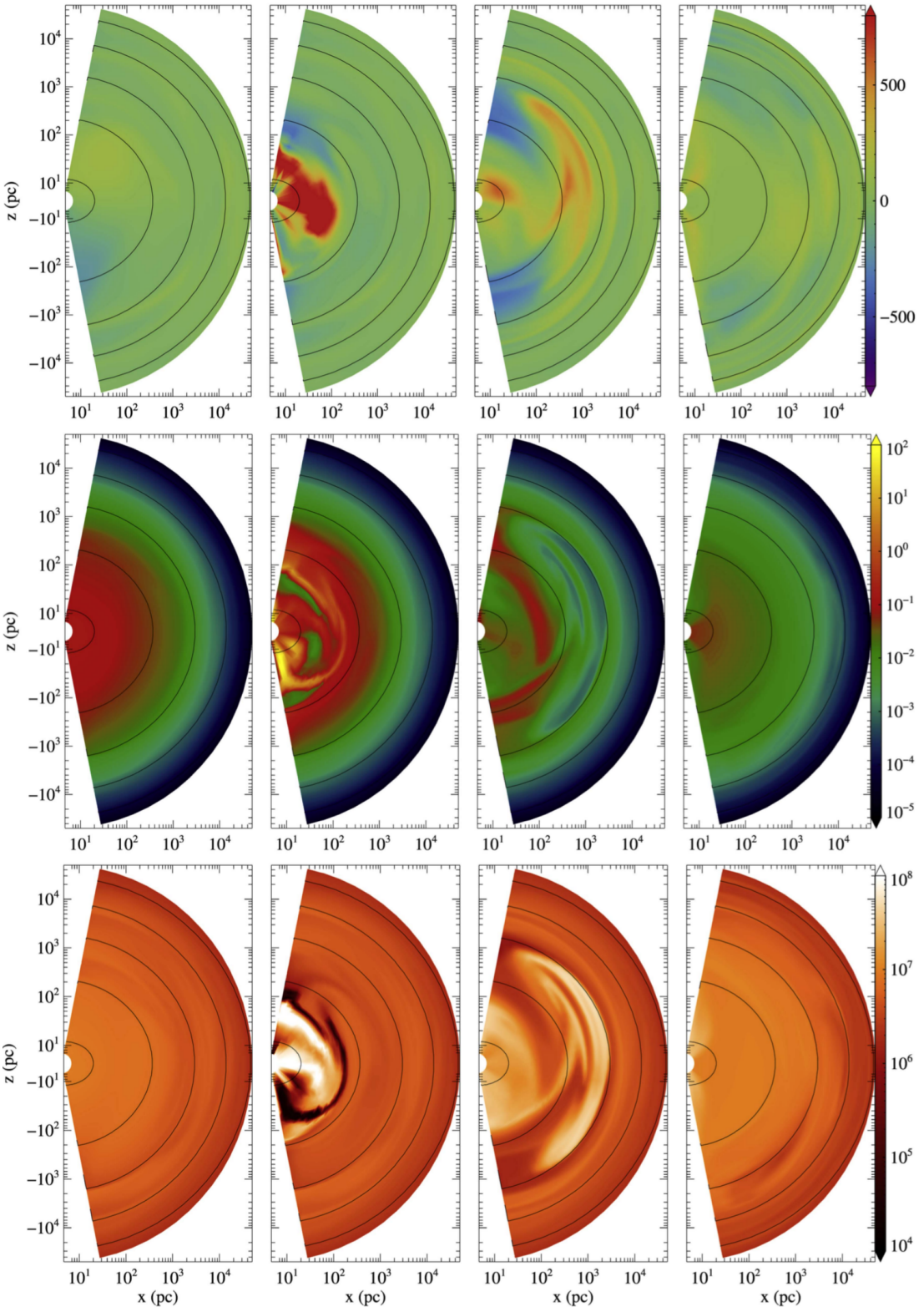

Figure 1.8: Top row: radial velocity field, in kms^{-1}; Central row: density field in cm^{-3}; bottom row: temperature field in K. There are four representative times in correspondance with an outburst at 6.85 Gyr. From left to right: $t = 6.84\ Gyr$, $t = 6.85\ Gyr$, $t = 6.86\ Gyr$ and $t = 6.95\ Gyr$. For detail see Ciotti, Pellegrini, et al. (2017).

The purpose of this thesis is to proceed towards a deeper understanding of radiative transfer in elliptical galaxies, in order to unveil the importance of radiative AGN feedback in galaxy evolution, its impact on the interstellar medium, and its role in determining the accreted mass on the central MBH.
The thesis is composed mainly by two parts:

In the first one we will show the analytical study of radiative transfer, and we will derive the moment equations for two different choices of the specific intensity function. We will show in detail the main equations of these models, which we will call *D Model* and *AD Model*. After that we will show the main differences between these models, both analytical and physical, and we will discuss the main implications of the uses of them.

In the second part we will investigate the physics of the ISM of Early-type Galaxies. Thus, we will study the impact on ISM by radiative AGN feedback, applying the D and the AD Models. We will show a detailed post processing study of the output hydro simulation (Ciotti, Pellegrini, et al. 2017), in which the radiative heating of ISM is firstly modelled by photoionization and transition line heating of partially ionized clouds; after that, we will add the presence of dust which absorbs radiation in UV and Optical bands. In the last section we will compare the AD Model with model used in Novak et al. (2012), that we will call N12 Model.

Finally we will discuss the pro and contra of the two models of radiative transfer, in the situations with and without dust.

Chapter 2

Radiative Transfer Modeling

2.1 Basics on Radiative Transfer

(Radiative transfer, S. Chandrasekhar (1950))

To set up the conditions of any problem concerning radiative transfer, we have to define some fundamental quantities (without losing generality, in this section we consider Cartesian coordinates):

We consider the radiant energy dE_ν in a specific frequency interval $(\nu, \nu + d\nu)$ which is

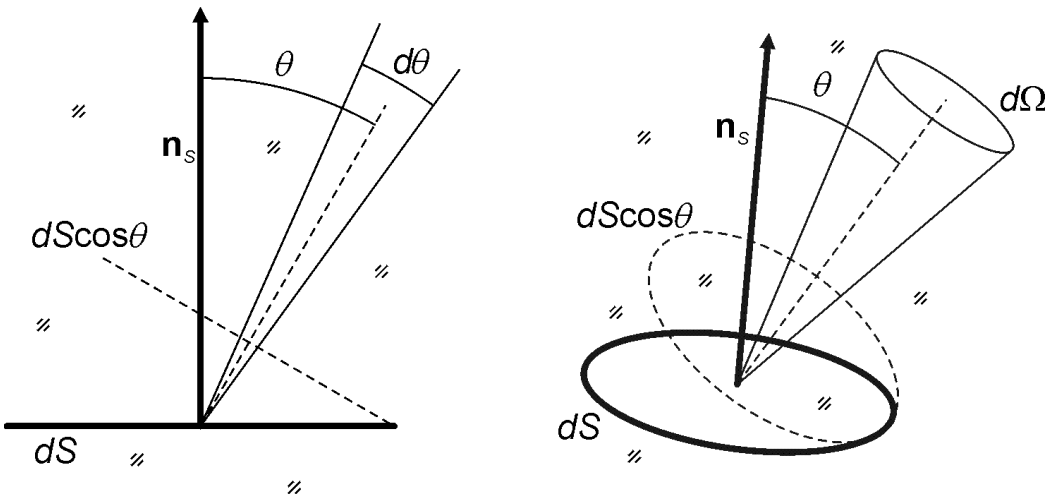

Figure 2.1: A "pencil of radiation".

transported across the area element dS and with a direction confined into the solid angle $d\Omega$, during a time dt. This energy is expressed in terms of *Specific Intensity* I_ν, which is given by

$$dE_\nu = I_\nu \cos\theta d\nu dS d\Omega dt \tag{2.1}$$

where θ is the angle whose direction is within the outward normal $\boldsymbol{n_s}$ to dS. The specific intensity thus defined is always $def > 0$. If we want to be mathematically strict we should write the 2.1 in the integral form, since dE is not a differential but it is a finite quantity of energy, and therefore greater than zero.

If we are in a medium which absorbs, emits and scatters radiation, I_ν can be expected to vary from point to point, from time to time and also with the direction through every point. Thus, we can write I_ν in Cartesian coordinates as:

$$I_\nu \equiv I_\nu(\boldsymbol{x}, \boldsymbol{n}, t) \tag{2.2}$$

where $\boldsymbol{x} = (x, y, z)$ defines the point and $\boldsymbol{n} = (l, m, n)$ defines the direction cosines of the direction to which I_ν refers.

In the 2.1 there is also dt, which implies the dependence on time: if we wanted to study this time-dependent problem we should write the relativistic equations for I_ν, and therefore they have to be Lorentz-invariant, since I_ν is generated by particles (photons) which travel at the speed of light.

In this work we study the stationary problem of radiative transfer applied to AGN feedback. We stress that we neglect the propagation time of photons which leave the central MBH to go outwards, because the light crossing time of the galaxy is by far the shortest time-scale of the system, so we can write the 2.2 as:

$$I_\nu \equiv I_\nu(\boldsymbol{x}, \boldsymbol{n}) \tag{2.3}$$

In other words, when the central source becomes luminous, photons propagate instantaneously in the whole galaxy. Moreover, if the specific intensity is independent of direction in a point, the radiation field is said *isotropic* in that point, and if it is the same for any point, the radiation field is said *homogeneous* and *isotropic*.

We call the *Integrated Intensity* I the specific intensity integrated over all the frequencies: $\int_0^\infty I_\nu d\nu$. The net flow in all directions is therefore given by:

$$d\nu dS dt \int I_\nu \cos\theta d\Omega \tag{2.4}$$

where the integration is over all solid angles. The quantity

$$F_\nu = \frac{1}{\pi} \int I_\nu \cos\theta d\Omega \tag{2.5}$$

is called *Net Flux* and it defines the rate of radiant energy flow across dS per unit area and

in the interval $(\nu, \nu+d\nu)$. Also F_ν depends on the direction of the outward normal to the elementary surface across which the flow has been considered; however, this dependence of the flux on direction is simple and it has vectorial nature.
We now define the amount of radiant energy per unit volume, in the frequency interval $(\nu, \nu+d\nu)$ at any given point, as the *energy density*, $u_\nu d\nu$. As for the integrated intensity, for the energy density we can also define:

$$u = \int_0^\infty u_\nu d\nu = \frac{1}{c}\int I d\Omega \tag{2.6}$$

It is often convenient to introduce the *average intensity*:

$$J_\nu = \frac{1}{4\pi}\int I_\nu d\Omega \tag{2.7}$$

which is related to the energy density by:

$$u_\nu = \frac{4\pi}{c} J_\nu \tag{2.8}$$

where c is the speed of light. If the specific intensity I_ν after traversing a thickness dl in the direction of its propagation becomes $I_\nu + dI_\nu$, then we can write:

$$\frac{dI_\nu}{I_\nu} = -\kappa_\nu \rho dl \tag{2.9}$$

where ρ is the density of the medium and κ_ν is defined as the *mass absorption coefficient* for radiation of frequency ν, and it is always positive. As it can be seen from the negative sign, dI_ν is always negative, thus if the radiation passes through an absorbing medium, the radiation will be always absorbed; however, this quantity can reappear in other directions as scattered radiation. Thus, we must distinguish between *true absorption* (κ_α) and *scattering* (κ_s).

The quantity on the right member of 2.9 gives the optical depth τ, which is a pure number, that is defined as:

$$\tau(s, s+ds) = \int_s^{s+ds} \kappa(s')\rho(s')ds' \ . \tag{2.10}$$

If the medium is *optically thin* ($\tau < 1$), the light we will not is absorbed to much; if the medium is *optically thick* ($\tau > 1$), photons are absorbed and re-emitted from the medium, as happens in stellar interiors.
As mentioned above, a medium can absorb, scatter, but it can also emit, so we have to define a source term of a general medium with a density ρ.
We define the *emission coefficient* j_ν, such that the amount of radiant energy is given by

$$dE_{em} = j_\nu dm d\Omega d\nu dt \tag{2.11}$$

which says that an element of mass dm emits this energy in a direction confined to an element of solid angle $d\Omega$, in the frequency interval $(\nu, \nu + d\nu)$ and in a time dt.

Now we have all terms which play a role in the fundamental equation of radiative transfer: the source terms (that include the "very" source terms, but also the "scattering" source terms) and the absorption terms:

$$< \nabla_{\boldsymbol{x}} I, \boldsymbol{n} >= \epsilon + \rho\kappa_s J - \rho(\kappa_\alpha + \kappa_s)I \tag{2.12}$$

where $\epsilon + \rho\kappa_s J$ are the source terms, and $\rho(\kappa_\alpha + \kappa_s)I$ is the absorption term.

Moreover, we have some terms which behave like source and absorption terms differently: as we have seen before, the $\rho\kappa_\alpha I$ term absorbs the intensity as written in 2.9; also the $\rho\kappa_s I$ is an absorption term, but the intensity of radiation which interacts with the medium is not really absorbed, but it is scattered isotropically. Finally the $\rho\kappa_s J$ is a source term, because it takes the specific intensity which is scattered from all the directions (precisely, J in 2.7) and that is added in the direction in which we are looking. To conclude, we will use the 2.12 in curvilinear coordinates (A.16), therefore in spherical coordinates, as shown in appendix A

$$\left[\frac{d}{d\lambda} I(\boldsymbol{r} + \lambda\boldsymbol{n}, \boldsymbol{n})\right]_{\lambda=0} = \mu\frac{\partial I}{\partial r} + \frac{1-\mu^2}{r}\frac{\partial I}{\partial \mu} \tag{2.13}$$

and therefore we finally obtain:

$$\mu\frac{\partial I}{\partial r} + \frac{1-\mu^2}{r}\frac{\partial I}{\partial \mu} = \rho\kappa_s J - \rho(\kappa_\alpha + \kappa_s)I + \epsilon \ . \tag{2.14}$$

The same result can be found in *Radiative Transfer*, S. Chandrasekhar (1950), where $\mu = \cos\theta$ and r is the radius.

2.2 The Radiative Transfer equations

We have derived the (strict) radiative transfer equation in curvilinear spherical coordinates.

$$\mu\frac{\partial I}{\partial r}+\frac{1-\mu^2}{r}\frac{\partial I}{\partial \mu}=-\rho(\kappa_\alpha+\kappa_s)I+\rho\kappa_s J+\epsilon \tag{2.15}$$

To find a solution for this equation we have to make a guess for the specific intensity function $I(r,\mu)$; we can start from the *Eddington Approximation*, which tells us that:

$$I(r,\mu)=A(r)+\mu B(r)\ . \tag{2.16}$$

In this case I is composed by two terms: $A(r)$ is the isotropic term, and $\mu B(r)$ is the mildly anisotropic term. This approximation is commonly adopted for the stellar interiors. In the stellar interior the medium is always optically thick for all photons from the centre to the photosphere, while the ISM of an ETG is generally in the optically thin regime, then we have to add a term which can quantify the opposite limit to $A(r)$, when the radiation field is highly directed (then, in the optically thin regime).
So doing the 2.16 becomes:

$$I(r,\mu)=A(r)+\mu B(r)+D(r)\delta(\mu-1) \tag{2.17}$$

The additional term $D(r)\delta(\mu-1)$ allows us to describe the central point-like quasar dominant for the radiation field where the specific intensity resembles that of a point source (the central MBH).
Now we take the moments in μ of order 0, 1 and 2 of I:

$$J\equiv\frac{1}{4\pi}\int_0^{2\pi}d\phi\int_{-1}^{1}I(\mu,\phi)d\mu=A+\frac{D}{4} \tag{2.18}$$

$$F\equiv\int_0^{2\pi}d\phi\int_{-1}^{1}\mu I(\mu,\phi)d\mu=\frac{4\pi B}{3}+\pi D \tag{2.19}$$

$$P\equiv\frac{1}{c}\int_0^{2\pi}d\phi\int_{-1}^{1}\mu^2 I(\mu,\phi)d\mu=\frac{4\pi A}{3c}+\frac{\pi D}{c} \tag{2.20}$$

and these are respectively the *mean intensity*, the *net energy flux* and the *radiation pressure*.We have taken the delta functions appearing at the edge of the integration domain to be equal to one-half in the above equations.

In the following we will derive the equations which can approximate the two asymptotic limits A and D (in other words, A, B and D tell us in which regime the medium is

for the radiation field) and, possibly, the intermediate regimes.
First we start taking the 2.15 and integrating it in $d\Omega$ one has:

$$\int_\Omega \mu \frac{\partial I}{\partial r} d\Omega + \int_\Omega \frac{1-\mu^2}{r} \frac{\partial I}{\partial \mu} d\Omega = -\int_\Omega \rho(\kappa_\alpha + \kappa_s) I d\Omega + \int_\Omega \rho \kappa_s J d\Omega + \int_\Omega \epsilon d\Omega \tag{2.21}$$

Integrating one by one all the terms of 2.21, then we have that the first term on the left member is

$$\int_\Omega \mu \frac{\partial I}{\partial r} d\Omega = \frac{\partial}{\partial r} \int_{-1}^{1} \mu I(\mu, \phi) d\mu = \frac{\partial F}{\partial r} \tag{2.22}$$

and the second term on the left member, integrating by parts, is:

$$\int_\Omega \frac{1-\mu^2}{r} \frac{\partial I}{\partial \mu} d\Omega = \frac{1}{r} \int_0^{2\pi} d\phi \left(\left[(1-\mu^2) I \right]_{-1}^{+1} - \int_{-1}^{1} -2\mu I d\mu \right) = \frac{2}{r} F \ . \tag{2.23}$$

We proceed on the right member, where the first term becomes

$$-\int_\Omega \rho(\kappa_\alpha + \kappa_s) I d\Omega = -\rho(\kappa_\alpha + \kappa_s) \int_0^{2\pi} d\phi \int_{-1}^{1} I(\mu, \phi) d\mu = -4\pi \rho(\kappa_\alpha + \kappa_s) J \tag{2.24}$$

and the second one is:

$$\int_\Omega \rho \kappa_s J d\Omega = 4\pi \rho \kappa_s J \tag{2.25}$$

and finally the last term is:

$$\int_\Omega \epsilon d\Omega = 4\pi \epsilon = \dot{E} \ . \tag{2.26}$$

We can simplify the right member

$$-4\pi(\rho\kappa_\alpha J - \rho\kappa_s J + \rho\kappa_s J) + \dot{E} = -4\pi\rho\kappa_\alpha J + \dot{E} \tag{2.27}$$

and in conclusion equation 2.21 becomes:

$$\frac{\partial F}{\partial r} = -\frac{2}{r} F - 4\pi\rho\kappa_\alpha J + \dot{E} \ . \tag{2.28}$$

Considering that

$$\frac{\partial F}{\partial r} + \frac{2}{r} F = \frac{1}{r^2} \left(\frac{\partial r^2 F}{\partial r} \right) \ , \tag{2.29}$$

we can rewrite the 2.28 as:

$$\frac{1}{r^2}(\frac{\partial r^2 F}{\partial r}) = -4\pi\rho\kappa_\alpha J + \dot{E} \ . \tag{2.30}$$

Using the relation between flux and luminosity in spherical symmetry:

$$F = \frac{L}{4\pi r^2} \tag{2.31}$$

we finally have

$$\frac{dL}{dr} = 4\pi r^2(\dot{E} - 4\pi\rho\kappa_\alpha J) \tag{2.32}$$

where the "∂" has become "d" in the derivative because L (and so also F) depends just on the radius r. The 2.28 and the 2.30 represent respectively how the flux and the luminosity vary while they're crossing the galaxy, our first equation to set up the problem of radiative transfer.
Next we take again the radiative transfer equation (2.15), we multiply it for μ and we integrate it in $d\Omega$, as we did before to obtain the 2.28:

$$\int_\Omega \mu^2 \frac{\partial I}{\partial r} d\Omega + \int_\Omega \frac{\mu - \mu^3}{r} \frac{\partial I}{\partial \mu} d\Omega = -\int_\Omega \mu\rho(\kappa_\alpha + \kappa_s) I d\Omega + \int_\Omega \mu\rho\kappa_s J d\Omega + \int_\Omega \mu\epsilon d\Omega \tag{2.33}$$

We integrate the whole equation (2.33), from the first term on the left member:

$$\int_\Omega \mu^2 \frac{\partial I}{\partial r} d\Omega = \frac{\partial}{\partial r} \int_0^{2\pi} d\phi \int_{-1}^{1} \mu^2 I(\mu, \phi) d\mu = \frac{\partial P}{\partial r} \ , \tag{2.34}$$

now taking the second term on the left member:

$$\frac{1}{c} \int_\Omega \frac{\mu - \mu^3}{r} \frac{\partial I}{\partial \mu} d\Omega = \frac{1}{rc} \int_0^{2\pi} d\phi \left(\left[(\mu - \mu^3) I \right]_{-1}^{+1} - \int (1 - 3\mu^2) I d\mu \right) \ , \tag{2.35}$$

and integrating it by parts we have:

$$\frac{1}{rc} \int_0^{2\pi} d\phi \left(- \int I d\mu + 3 \int \mu^2 I d\mu \right) = -\frac{4\pi J}{rc} + \frac{3P}{r} \ . \tag{2.36}$$

We integrate the first term on the right member:

$$-\frac{1}{c} \int_\Omega \mu\rho(\kappa_\alpha + \kappa_s) I d\Omega = -\frac{\rho(\kappa_\alpha + \kappa_s)}{c} \int_0^{2\pi} d\phi \int_{-1}^{1} \mu I d\mu = -\frac{\rho(\kappa_\alpha + \kappa_s) F}{c} \ , \tag{2.37}$$

and finally we show that the last two terms on the right vanish:

$$\frac{1}{c}\int_{\Omega}\mu\rho\kappa_s J d\Omega = \frac{1}{c}\int_0^{2\pi} d\phi \int_{-1}^{1}\mu\rho\kappa_s J d\mu = 0 \ , \tag{2.38}$$

because J does not depend on μ, and

$$\frac{1}{c}\int_{\Omega}\mu\epsilon d\Omega = \frac{1}{c}\int_0^{2\pi} d\phi \int_{-1}^{1}\mu\epsilon d\mu = 0 \ , \tag{2.39}$$

because ϵ is isotropic. In the last three expressions we have multiplied for $\frac{1}{c}$ for dimensional physics reasons.
Combining all the results above, we finally have:

$$\frac{dP}{dr} + \frac{3P}{r} = +\frac{4\pi J}{rc} - \frac{\rho\kappa_t F}{c} \tag{2.40}$$

where $\kappa_t = \kappa_\alpha + \kappa_s$, and where we have changed $\partial \mapsto d$ because of the only dependence on r.
We now have all the ingredients to investigate the problem of radiative transfer: the 3 moments of I in μ:

$$J = A + \frac{D}{4} \tag{2.41}$$

$$F = \frac{4\pi B}{3} + \pi D \tag{2.42}$$

$$P = \frac{4\pi A}{3c} + \frac{\pi D}{c} \tag{2.43}$$

and the two equations obtained as moments of the radiative transfer equation:

$$\frac{dF}{dr} = -\frac{2}{r}F - 4\pi\rho\kappa_\alpha J + \dot{E} \tag{2.44}$$

$$\frac{dP}{dr} + \frac{3P}{r} = +\frac{4\pi J}{rc} - \frac{\rho\kappa_t F}{c} \ . \tag{2.45}$$

In the following we investigate the implications of our choice for the expression for I in equation 2.17, that is flexible enough to allow us to switch from an optically thick regime

(dominated by the "A" term) to an optically thin regime (dominated by the "D" term, i.e. with a dominant central point source, the central MBH). We mainly explore two models: the first one is the "D Model", used in Ciotti, Pellegrini, et al. (2017), which treats the ISM as a quasi-optically thin medium. The second one is the "AD Model", that is used in this thesis work, that will be explored in depth afterwards.

2.3 The D Model

The choice of the intensity function for this model is simply:

$$I(r,\mu) = D(r)\delta(\mu - 1) \tag{2.46}$$

With this choice, the three moments 2.41-2.43, with the terms A and B equal to zero, become:

$$J = \frac{D}{4} \tag{2.47}$$

$$F = \pi D \tag{2.48}$$

$$P = \frac{\pi D}{c} \ . \tag{2.49}$$

Taking the 2.28:

$$\frac{dF(r)}{dr} + \frac{2}{r}F(r) = -4\pi\rho(r)\kappa_\alpha(r)J(r) + \dot{E}(r) \tag{2.50}$$

and writing it as a function of D, we have:

$$\pi\frac{dD(r)}{dr} + \frac{2\pi}{r}D(r) = -\pi\rho(r)\kappa_\alpha(r)D(r) + 4\pi\epsilon(r) \tag{2.51}$$

that is:

$$\frac{dD(r)}{dr} + \frac{2}{r}D(r) = 4\epsilon(r) - \rho(r)\kappa_\alpha(r)D(r) \ . \tag{2.52}$$

Knowing that :

$$L = 4\pi r^2 F = 4\pi^2 r^2 D \tag{2.53}$$

and

$$\frac{dD}{dr} + \frac{2}{r}D = \frac{1}{r^2}\frac{d(r^2 D)}{dr} \ , \tag{2.54}$$

we can write 2.44 as:

$$\frac{dL(r)}{dr} = 4\pi r^2 \dot{E}(r) - \rho(r)\kappa_\alpha(r)L(r) \ . \tag{2.55}$$

If there are not discrete energy sources (like star formation input energy), then $\dot{E} = 0$

and we have

$$\frac{dL(r)}{dr} = -\rho(r)\kappa_\alpha(r)L(r) \ . \tag{2.56}$$

Equation 2.56 tells us that in a general absorbing medium (with $\kappa_\alpha > 0$) we have that $\frac{dL}{dr} < 0$, thus the light decreases with increasing radius.
Once we have the net flux F (2.48), for the 2.50 the radiation pressure is simply

$$P = \frac{F}{c} \ . \tag{2.57}$$

To find ∇P, let's take the 2.45:

$$\frac{dP(r)}{dr} = -\frac{3P(r)}{r} + \frac{4\pi J(r)}{rc} - \frac{\rho(r)\kappa_t(r)F(r)}{c} \tag{2.58}$$

we insert P and J, and taking into account the 2.53 we can write

$$\frac{dP(r)}{dr} = -\left(\frac{2L(r)}{4\pi r^3 c} + \frac{\rho(r)\kappa_\alpha(r)L(r)}{4\pi r^2 c}\right)\boldsymbol{e_r} \ . \tag{2.59}$$

We have the same result for the electron scattering, with the difference that the light is never absorbed, so we have

$$\left(\frac{dP(r)}{dr}\right)_{es} = -\left(\frac{2L(r_0)}{4\pi r^3 c} + \frac{\rho(r)\kappa_{es}L(r_0)}{4\pi r^2 c}\right)\boldsymbol{e_r} \ . \tag{2.60}$$

The inner boundary condition $L(r_0)$ is equal to L_{BH} (for this type of problem), defined as:

$$L_{BH} = \epsilon_{em}\dot{M}_{bh}c^2 \tag{2.61}$$

where ϵ_{em} is the radiative electromagnetic efficiency, $\dot{M}_{bh}$ is the mass accretion rate onto the MBH.

2.4 The AD Model

The choice for the intensity function for this model is a little more complicated:

$$I(r,\mu) = A(r) + D(r)\delta(\mu - 1) \ . \tag{2.62}$$

With this choice, the three moments J, F and P in 2.41-2.43 become:

$$J = A + \frac{D}{4} \tag{2.63}$$

$$F = \pi D \tag{2.64}$$

$$P = \frac{4\pi A}{3c} + \frac{\pi D}{c} \tag{2.65}$$

where we have put the mildly-anisotropic term $B = 0$. Considering the first equation in F (2.28)

$$\frac{dF}{dr} = -\frac{2}{r}F - 4\pi\rho\kappa_\alpha J + \dot{E} \tag{2.66}$$

we rewrite this equation in terms of D and A, which indicates how the radiation field is isotropic or direct:

$$\pi\frac{dD(r)}{dr} = -\frac{2\pi}{r}D(r) - 4\pi\rho(r)\kappa_\alpha(r)\left(A(r) + \frac{D(r)}{4}\right) + \dot{E}(r) \ . \tag{2.67}$$

We simplify and we have the first equation for the AD Model:

$$\frac{dD(r)}{dr} + \frac{2D(r)}{r} = \frac{\dot{E}(r)}{\pi} - 4\rho(r)\kappa_\alpha(r)\left(A(r) + \frac{D(r)}{4}\right) \ . \tag{2.68}$$

Now let's take the second equation in P (2.45):

$$\frac{dP(r)}{dr} + \frac{3P(r)}{r} = \frac{4\pi J(r)}{rc} - \frac{\rho(r)\kappa_t(r)F(r)}{c} \tag{2.69}$$

and as we did for the first equation, we rewrite it in terms of D and A

$$\frac{d}{dr}\left(\frac{4\pi A(r)}{3c} + \frac{\pi D(r)}{c}\right) + \frac{3}{r}\left(\frac{4\pi A(r)}{3c} + \frac{\pi D(r)}{c}\right) = \frac{4\pi}{rc}\left(A(r) + \frac{D(r)}{4}\right) - \frac{\rho(r)\kappa_t(r)\pi D(r)}{c} \ . \tag{2.70}$$

Then we multiply it for $\frac{3c}{4\pi}$ and we simplify

$$\frac{3}{4}\frac{dA(r)}{dr} + \frac{dD(r)}{dr} + \frac{2D(r)}{r} = -\rho(r)\kappa_t(r)D(r) \tag{2.71}$$

we insert the 2.68 into the 2.71:

$$\frac{3}{4}\frac{dA(r)}{dr} + \frac{\dot{E}(r)}{\pi} - 4\rho(r)\kappa_\alpha(r)\left(A(r) + \frac{D(r)}{4}\right) = -\rho(r)\kappa_a(r)D(r) - \rho(r)\ ,\kappa_s D(r) \tag{2.72}$$

we simplify

$$\frac{3}{4}\frac{dA(r)}{dr} = 4\rho\kappa_\alpha A(r) - \rho(r)\kappa_s D(r) - \frac{\dot{E}(r)}{\pi} \tag{2.73}$$

and we finally obtain:

$$\frac{dA(r)}{dr} = 3\rho(r)\left(\kappa_\alpha(r)A(r) - \kappa_s\frac{D(r)}{4}\right) - \frac{3\dot{E}(r)}{4\pi}\ . \tag{2.74}$$

We now have two equations in two unknowns:

$$\frac{dD(r)}{dr} + \frac{2}{r}D(r) = \frac{\dot{E}(r)}{\pi} - 4\rho(r)\kappa_\alpha(r)\left(A(r) + \frac{D(r)}{4}\right) \tag{2.75}$$

$$\frac{dA(r)}{dr} = 3\rho(r)\left(\kappa_\alpha(r)A(r) - \kappa_s\frac{D(r)}{4}\right) - \frac{3\dot{E}(r)}{4\pi} \tag{2.76}$$

where we can see the term "A" like an isotropization term.

It is important to understand that the "A equation" (2.76) must be integrated, as the majority of the radiative transfer problems, from $+\infty$ to 0 because we do not know the central boundary condition, and the "D equation" (2.136) from 0 to $+\infty$, as we will see in section 2.5.

The inner boundary condition for D and A derive, as in the D Model, from the central L_{BH}:

$$D(r_0) = \frac{F(r_0)}{\pi} = \frac{L_{BH}}{4\pi^2 r_0^2}\ , \tag{2.77}$$

because the light is all-directed from the central MBH at the initial radius; for this reason

$$A(r_0) = 0\ . \tag{2.78}$$

We can see also how, despite the radiation originated from the central point source has a radial direction, the medium tends to make it isotropic. Thus, it is very important to understand how radiation changes depending on the ISM conditions (i.e. the hydrodynamics, chemical composition, etc).

To find ∇P we proceed as in section 2.3, we take the 2.45:

$$\frac{dP(r)}{dr} = -\frac{3P(r)}{r} + \frac{4\pi J(r)}{rc} - \frac{\rho(r)\kappa_t(r)F(r)}{c} \tag{2.79}$$

we insert P and J and, taking in account the 2.53, we have:

$$\frac{dP(r)}{dr} = -\left(\frac{2L(r)}{4\pi r^3 c} + \frac{\rho(r)\kappa_\alpha(r)L(r)}{4\pi r^2 c}\right)\boldsymbol{e_r} \tag{2.80}$$

and for the electron scattering:

$$\left(\frac{dP(r)}{dr}\right)_{es} = -\left(\frac{2L(r_0)}{4\pi r^3 c} + \frac{\rho(r)\kappa_{es}L(r_0)}{4\pi r^2 c}\right)\boldsymbol{e_r}\ . \tag{2.81}$$

The expression for ∇P in the AD Model is the same as for ∇P of the D Model, but it can have some differences caused by the variation of $L_{BH}^{eff}(r)$. We will investigate this topic in chapter 4.

2.5 Closed Form of the AD Equations

In this section we search for an integral, closed form of the A and D equations, which will allow us to understand some interesting and deep properties of the two functions $A(r)$ and $D(r)$ of the AD model.
First of all, we rewrite them :

$$\frac{dD(r)}{dr} + \frac{2}{r}D(r) = \frac{\dot{E}(r)}{\pi} - 4\rho(r)\kappa_\alpha(r)\left(A(r) + \frac{D(r)}{4}\right) \tag{2.82}$$

$$\frac{dA(r)}{dr} = 3\rho(r)\left(\kappa_\alpha(r)A(r) - \kappa_s\frac{D(r)}{4}\right) - \frac{3\dot{E}(r)}{4\pi} \ . \tag{2.83}$$

In our scheme, the directional part of the intensity $D(r)\delta(\mu - 1)$ cannot be negative, because we are studying only photons which "escape" from the central MBH; also the isotropic part of the intensity $A(r)$ is necessarily greater than zero, as shown below.

We know, for the definition of intensity, that $I(r, \mu) \geq 0$; we suppose that $A(r) < 0$ and in the μ direction we have that $I(r, \mu) = A(r) + D(r)\delta(\mu - 1) > 0$; so if we move at fixed radius of an angle from μ, the δ function becomes zero, $A(r)$ does not depend on μ, and $I(r, \mu) < 0$ as a consequence. So the isotropic term cannot be less than zero.
Let's see another example:
Taking the AD equations and considering that $\dot{E}(r) = 0$, they become:

$$\frac{dD(r)}{dr} + \frac{2}{r}D(r) = -4\rho(r)\kappa_\alpha(r)\left(A(r) + \frac{D(r)}{4}\right) \tag{2.84}$$

$$\frac{dA(r)}{dr} = 3\rho(r)\left(\kappa_\alpha(r)A(r) - \kappa_s\frac{D(r)}{4}\right) \tag{2.85}$$

Suppose that in a certain radius r_n we have $D(r_n) = 0$: we can see from the 2.84 that we would have $D(r_n) + dD(r) < 0$, which is impossible in our scheme, so if $D(r_n) = 0$, also $A(r_n) = 0$.

On the other hand, if we have $A(r_n) = 0$ and $D(r_n) > 0$, we can see from the 2.85 that we can have $A(r_n) + dA(r) < 0$, which is impossible too. We can conclude that, if we have $D(r_n) = 0$, also $A(r_n) = 0$ and vice versa.

Another important property is that if exists $D(r_n) \neq 0$ then $\lim_{r\to\infty} D(r) = 0$ and exists an scattering coefficient opacity $\kappa_s \neq 0$, then exists $A(r_n) \neq 0$ and $\lim_{r\to\infty} A(r) = 0$.

To better understand these and other properties, in the next sections we are going to find a closed form for these two equations (for the sake of simplicity, we will put $\dot{E} = 0$) using the method of the variation of parameters, also known as variation of constants.

2.5.1 Integration of the D Equation

We start writing the differential equation for $D(r)$:

$$\frac{dD(r)}{dr} + \frac{2D(r)}{r} = -4\rho(r)\kappa_\alpha(r)A(r) - \rho(r)\kappa_\alpha(r)D(r) \tag{2.86}$$

and rewrite it in another form, to integrate it easily:

$$\frac{1}{r^2}\left(\frac{dr^2D(r)}{dr}\right) = -4\rho(r)\kappa_\alpha(r)A(r) - \rho(r)\kappa_\alpha(r)D(r)\ . \tag{2.87}$$

Then we multiply the two members for 4π, and using the 2.53 we have:

$$\frac{dL(r)}{dr} = -16\pi^2\rho(r)\kappa_\alpha(r)r^2A(r) - \rho(r)\kappa_\alpha(r)L(r)\ . \tag{2.88}$$

We define two new functions $f(r)$ and $g(r)$:

$$f(r) = -\rho(r)\kappa_\alpha(r) \tag{2.89}$$

$$g(r) = 16\pi^2\rho(r)\kappa_\alpha(r)r^2A(r) \tag{2.90}$$

and finally, we write the 2.88 as:

$$\frac{dL(r)}{dr} = f(r)L(r) - g(r)\ . \tag{2.91}$$

We intend to find a solution for this homogeneous equation, so with $g(r) = 0$,

$$L_0'(r) = fL_0(r)\ , \tag{2.92}$$

$$\frac{L_0'(r)}{L_0(r)} = f(r) \longrightarrow ln\left(\frac{L_0(r)}{L_0(r_1)}\right) = \int_{r_1}^{r} f(t)dt = F(r, r_1)\ . \tag{2.93}$$

The homogeneous solution for the 2.91 is:

$$L_0(r) = L_0(r_1)e^{F(r,r_1)} \tag{2.94}$$

the general solution of 2.88 (which is non homogeneous) it is like that:

$$L_1'(r) = L_0(r)u(r) \tag{2.95}$$

so deriving the second member and making it equal to the second member of 2.88, we have:

$$L_0'(r)u(r) + L_0(r)u'(r) = f(r)L_0(r)u(r) - g(r) \ , \tag{2.96}$$

$$u(r)(L_0' - f(r)L_0) + L_0u'(r) = -g(r) \tag{2.97}$$

with $L_0' = f(r)L_0$ from the 2.92, and using the 2.94, we write :

$$u'(r) = -\frac{g(r)}{L_0} \quad \longrightarrow \quad u(r) = -\frac{g(r)}{L_0(r_1)}e^{F(r,r_1)} \tag{2.98}$$

with $r_1 \neq r$. We know that

$$L_0(r_0) = L_{BH} \ . \tag{2.99}$$

We write the most general solution of D equation:

$$L(r_0) = L_0(r_0) + L_1(r_0) = L_0(r_0)[1 + u(r_0)] \ , \tag{2.100}$$

in this case we have $u(r_0) = 0$ and we can write :

$$u(r_0) = u(r_2) - \frac{1}{L_0(r_1)}\int_{r_2}^{r_0} g(x)e^{-F(x,r_1)}dx = 0 \tag{2.101}$$

with $r_2 \neq r$ and $r_2 \neq r_1$,

$$u(r_2) = \frac{1}{L_0(r_1)}\int_{r_2}^{r_0} g(x)e^{-F(x,r_1)}dx \ . \tag{2.102}$$

Let's write the non homogeneous solution for a generic radius, starting from the 2.100 and substituting $u(r_2)$ with the 2.102, we obtain:

$$L(r) = L_0(r)[1 + u(r)] = L_0(r)\left[1 + u(r_2) - \frac{1}{L_0(r_1)}\int_{r_2}^{r_0} g(x)e^{-F(x,r_1)}dx\right] \tag{2.103}$$

and then,

$$L(r) = \left[1 + \frac{1}{L_0(r_1)}\int_{r_2}^{r_0} g(x)e^{-F(x,r_1)}dx - \frac{1}{L_0(r_1)}\int_{r_2}^{r_0} g(x)e^{-F(x,r_1)}dx\right] . \tag{2.104}$$

We can change the sign of the last part of the second member reversing the extremes of

the integral

$$-\frac{1}{L_0(r_1)}\int_{r_1}^{r_0} g(x)e^{-F(x,r_1)}dx = \frac{1}{L_0(r_1)}\int_{r_0}^{r_1} g(x)e^{-F(x,r_1)}dx \tag{2.105}$$

so, the 2.100 becomes:

$$L(r) = L_0(r)\left[1 - \frac{1}{L_0(r_1)}\int_{r_0}^{r} g(x)e^{-F(x,r_1)}dx\right] = L_0(r) - \frac{L_0(r)}{L_0(r_1)}\int_{r_0}^{r} g(x)e^{-F(x,r_1)}dx \tag{2.106}$$

and finally we obtain:

$$L(r) = L_0(r) - \int_{r_0}^{r} g(x)e^{F(r,r_1)-F(x,r_1)}dx\ . \tag{2.107}$$

We can rearrange the exponent appearing in the integral

$$F(r,r_1)-F(x,r_1) = \int_{r_1}^{r} f(t)dt - \int_{r_1}^{x} f(t)dt = \int_{r_1}^{r} f(t)dt + \int_{x}^{r_1} f(t)dt = F(r,x)\ , \tag{2.108}$$

so finally the solution is:

$$L(r) = L_0(r_0) - \int_{r_0}^{r} g(x)e^{F(r,x)}dx\ . \tag{2.109}$$

Let's substitute $f(r)$ and $g(r)$ using 2.89 and 2.90:

$$L(r) = L_0(r) - 16\pi^2\int_{r_0}^{r} \rho(x)\kappa_\alpha(x)x^2A(x)e^{-\int_x^r \rho(t)\kappa_\alpha(t)dt}dx \tag{2.110}$$

and knowing that

$$L(r) = 4\pi^2r^2D(r)\ , \tag{2.111}$$

we finally write the general solution for $L(r)$:

$$L(r) = L_{BH}e^{-\int_{r_0}^r \rho(t)\kappa_\alpha(t)dt} - 16\pi^2\int_{r_0}^{r} \rho(x)\kappa_\alpha(x)x^2A(x)e^{-\int_x^r \rho(t)\kappa_\alpha(t)dt}dx \tag{2.112}$$

we can write the final solution for the $D(r)$ equation using 2.99 and 2.111

$$D(r) = D(r_0)\left(\frac{r}{r_0}\right)^{-2}e^{-\int_{r_0}^r \rho(t)\kappa_\alpha(t)dt} - \frac{4}{r^2}\int_{r_0}^{r} \rho(x)\kappa_\alpha(x)x^2A(x)e^{-\int_x^r \rho(t)\kappa_\alpha(t)dt}dx \tag{2.113}$$

with

$$D(r_0) = \frac{L_{BH}}{4\pi^2r_0^2}\ . \tag{2.114}$$

2.5.2 Integration of the A Equation

Let's start writing the differential equation for $A(r)$:

$$\frac{dA(r)}{dr} = 3\rho(r)\kappa_\alpha(r)A(r) - \frac{3}{4}\rho(r)\kappa_s(r)D(r) \ ; \tag{2.115}$$

as we have done for the differential equation for $D(r)$, we are going to define two new functions $f(r)$ and $g(r)$:

$$f(r) = 3\rho(r)\kappa_\alpha(r) \ , \tag{2.116}$$

$$g(r) = \frac{3}{4}\rho(r)\kappa_s D(r) \ , \tag{2.117}$$

and we write the differential equation for $A(r)$ in terms of $f(r)$ and $g(r)$:

$$\frac{dA(r)}{dr} = f(r)A(r) - g(r) \ . \tag{2.118}$$

We're going to find the homogeneous solution of 2.118, so with $g(r) = 0$

$$\frac{A_0'(r)}{A_0(r)} = f(r) \quad \longrightarrow \quad ln\left(\frac{A_0(r)}{A_0(r_1)}\right) = \int_{r_1}^{r} f(t)dt = F(r, r_1) \tag{2.119}$$

so the general solution for $A(r)$ is:

$$A_0(r) = A_0(r_1)e^{F(r,r_1)} \tag{2.120}$$

with $r_1 \neq r$. The general solution of 2.118 is like that:

$$A_1(r) = A_0(r)u(r) \ ; \tag{2.121}$$

we derive the second member of 2.121 and making it equal to the second member of 2.118:

$$A_0'(r)u(r) + A_0(r)u'(r) = f(r)A_0(r)u(r) - g(r) \tag{2.122}$$

$$u(r)(A_0' - f(r)A_0) + A_0u'(r) = -g(r) \ , \tag{2.123}$$

knowing that $A_0' = f(r)A_0$ from the 2.119, we can write:

$$u'(r) = -\frac{g(r)}{A_0(r)} \ , \tag{2.124}$$

and integrating it, with $r_2 \neq r$ and $r_2 \neq r_1$, we obtain:

$$u(r) = u(r_2) - \frac{1}{A_0(r_1)} \int_{r_2}^{r} g(x) e^{-F(x,r_1)} dx \ . \tag{2.125}$$

We know that $\exists\, r_m$ such that $A(r_m) = D(r_m) = 0$, and we put ourselves in this boundary condition ,

$$A(r_m) = A_0(r_m) + A_1(r_m) = A_0(r_m)[1 + u(r_m)] \ , \tag{2.126}$$

so that :

$$A(r_m) = 0 \iff 1 + u(r_m) = 0 \ . \tag{2.127}$$

Integrating it from r_m to a generic radius $r < r_m$

$$1 + u(r_m) = u(r_2) - \frac{1}{A_0(r_1)} \int_{r_2}^{r} g(x) e^{-F(x,r_1)} dx + 1 = 0 \tag{2.128}$$

$$u(r_2) = \frac{1}{A_0(r_1)} \int_{r_2}^{r} g(x) e^{-F(x,r_1)} dx - 1 \ , \tag{2.129}$$

from 2.126 and 2.127 we write :

$$A(r) = A_0(r)[1 + u(r)] = A_0(r) \left[1 + u(r_2) - \frac{1}{A_0(r_1)} \int_{r_2}^{r} g(x) e^{-F(x,r_1)} dx \right] \ , \tag{2.130}$$

substituting $u(r_2)$ with the 2.129, we obtain:

$$A(r) = A_0(r) \left[\frac{1}{A_0(r_1)} \int_{r_2}^{r} g(x) e^{-F(x,r_1)} dx - \frac{1}{A_0(r_1)} \int_{r_2}^{r} g(x) e^{-F(x,r_1)} dx \right] \tag{2.131}$$

$$\frac{A_0(r)}{A_1(r)} \int_{r}^{r_m} g(x) e^{-F(x,r_1)} = e^{F(r,r_1)} \int_{r}^{r_m} g(x) e^{-F(x,r_1)} = \int_{r}^{r_m} g(x) e^{F(r,r_1) - F(x,r_1)} \ . \tag{2.132}$$

We can rearrange the exponent into the integral as we have done in section 2.5.1

$$F(r,r_1)-F(x,r_1)=\int_{r_1}^{r} f(t)dt-\int_{r_1}^{x} f(t)dt=\int_{r_1}^{r} f(t)dt+\int_{x}^{r_1} f(t)dt=F(r,x)\ , \quad (2.133)$$

and we finally have the general solution for $A(r)$:

$$A(r)=\int_{r}^{r_m} g(x)e^{F(r,x)}dx\ , \quad (2.134)$$

and using the 2.116 and 2.117 we finally have :

$$A(r)=\frac{3\kappa_s}{4}\int_{r}^{r_m} \rho(r)D(r)e^{3\int_{x}^{r_m}\rho(t)\kappa_\alpha(t)dt}dx\ . \quad (2.135)$$

2.6 Discussion

We've seen previously that it is very important to choose a consistent form for the intensity: in section 2.3, for the D Model we have seen that we have just one differential equation to integrate, from the central boundary to outside:

$$\frac{dD(r)}{dr} + \frac{2D(r)}{r} = \dot{E}(r) - \rho(r)\kappa_\alpha(r)D(r) \ . \tag{2.136}$$

The only type of opacity in this differential equation is the so called "true" absorption opacity, and not the scattering opacity; so we can say that the approximation which we choose for the intensity $I(r,\mu) = D(r)\delta(1-\mu)$ is a good approximation for an optically thin regime, without the presence of scattering from any kind of particle.

In section 2.4 we have seen that, adding an isotropic term $A(r)$ to the intensity, we have two equations which must be integrate in two different ways:

$$\frac{dD(r)}{dr} + \frac{2D(r)}{r} = \frac{\dot{E}(r)}{\pi} - 4\rho(r)\kappa_\alpha(r)\left(A(r) + \frac{D(r)}{4}\right) \tag{2.137}$$

$$\frac{dA(r)}{dr} = 3\rho(r)\left(\kappa_\alpha(r)A(r) - \kappa_s\frac{D(r)}{4}\right) - \frac{3\dot{E}(r)}{4\pi} \ . \tag{2.138}$$

The first one (2.137) is a differential equation that we have to integrate, as we have seen for the 2.136, from the central boundary to the external radius. We can see some differences between the equation for $D(r)$ with the two approximations: in the second case we have an additional term which participates in the absorption of the radiative (collimated) field. In some ways, the more we have the isotropic term, the more the direct radiative field is absorbed.

In the second one (2.138) we have a differential equation for $A(r)$, which has to be integrated from the outer radius to the central boundary condition of the $D(r)$ differential equation; we can imagine a trend of this equation changing its sign, so we have two source terms which are $\frac{3\dot{E}(r)}{4\pi}$ and $\frac{3}{4}\kappa_s\rho(r)D(r)$ and one absorbing term, $3\rho(r)\kappa_\alpha(r)A(r)$.

In this work we look for a good modeling for the AGN radiative feedback, so with $\dot{E} = 0$; when there is an AGN outburst, the AGN luminosity starts from the MBH only with the direct radiative field, that is $D(r)$, and with $A(r) = 0$. The 2.138 tells us that if we start with only direct radiation, the term $\rho(r)\kappa_s\frac{3D(r)}{4}$ generates the isotropic radiation $A(r)$ with the presence of a scattering medium. In early-type galaxies there can be a large amount of hot gas, as a consequence, we expect a large fraction of free electrons, which scatters light. To sum up, the approximation of the 2.4 seems more fit for the problem dealt with in our work, so now we are going to focus on the AD model.

In sections 2.5.1 and 2.5.2 we have seen that it is possible to find a closed form for the two equations 2.137 and 2.138; Here we repeat the solution to 2.137:

$$D(r) = D(r_0)\left(\frac{r}{r_0}\right)^{-2} e^{-\int_{r_0}^{r}\rho(t)\kappa_\alpha(t)dt} - \frac{4}{r^2}\int_{r_0}^{r}\rho(x)\kappa_\alpha(x)x^2A(x)e^{-\int_{x}^{r}\rho(t)\kappa_\alpha(t)dt}dx \quad (2.139)$$

In general the equation can be written in terms of the optical depth (2.10):

$$D(r) = D(r_0)\left(\frac{r}{r_0}\right)^{-2} e^{-\tau_\alpha(r,r_0)} - \frac{4}{r^2}\int_{r_0}^{r}\rho(x)\kappa_\alpha(x)x^2A(x)e^{-\tau_\alpha(r,x)}dx \quad (2.140)$$

The first term describes how much the medium absorbs the direct radiation field, which is expressed in terms of radiation flux, because of the r^{-2}. The second one shows us that the isotropic part of the radiation field generated from the scattering is absorbed from the medium, as well as the direct radiation field is absorbed.
Now we consider the solution for $A(r)$:

$$A(r) = \frac{3\kappa_s}{4}\int_{r}^{r_m}\rho(r)D(r)e^{3\int_{x}^{r_m}\rho(t)\kappa_\alpha(t)dt}dx \ ; \quad (2.141)$$

Also in this case we can write the equation for $A(r)$ in terms of $\tau(r, r')$:

$$A(r) = \frac{3\kappa_s}{4}\int_{r}^{r_m}\rho(r)D(r)e^{3\tau_\alpha(r_m,x)}dx \ . \quad (2.142)$$

First of all, we can see that if $k_s = 0$, there is not generation of isotropic radiation field; thus, in presence of a scattering medium, we must use the AD model approximation, to be consistent with the physics inside the ISM. Furthermore, since we have to integrate from r_m to r with $r_m > r$, the equation shows that the isotropic component of the radiation field at radius r depends on the radiation "back-scattered" from the interaction of the direct radiation field with the medium, which can absorb as well as scatter.

Chapter 3

The Interstellar Medium of Early-type Galaxies

In the last four decades the observations of very energetic radiation from MBHs at cosmological distances have drawn our attention, so, it's very important to constrain the input energy radiation for the central MBHs of galaxies, with which try to model the radiative feedback on ISM.

In this section we will show the condition of the ISM surrounding the central MBH of elliptical galaxies and the phenomena that transport energy and momentum from the radiation to the ISM. In the first part we are talking about the impact of radiation on *cold*, *warm* and hot gas ($T \leq few \cdot 10^7\ K$) in terms of *Compton* and *photoionization* heating using the equations in Sazonov, Ostriker, Ciotti, et al. (2005); in the second part we are going to add the presence of *dust* to explorate radiative transfer in obscured quasars, following the treatment of dust in Ciotti and Ostriker (2007).
In both cases (gas and dust) we use the characteristic angular-integrated, broad-band spectral energy distribution of the average quasar in the universe computed in Sazonov, Ostriker, and Sunyaev (2004) and used in Ciotti and Ostriker (2007).

The maps of hydrodynamics quantities in this section are computed using the results of the simulations in Ciotti, Pellegrini, et al. (2017) of an elliptical galaxy E4 with a total mass of $M \sim 3 \cdot 10^{12} M_{\odot}$, with a modified version of the parallel ZEUS code (Hayes et al. (2006)), in a 2D axisymmetric configuration, with a radially logarithmic grid in spherical coordinates (r, θ) of 128×32 meshpoints, spanning from 2.5 pc to 250 kpc, starting from an age of 2 Gyr, with a reflecting boundary conditions that is set along the z-axis, while at the outer edge of the computational domain the fluid is free to flow out.

For all the maps that we will show in this and in the next chapters, the z-axis was excluded in order to avoid gas sticking on it, due to the singularity of the coordinates on the z-axis. In the white zone inside $\sim 2.5\ pc$ nothing is computed, because that is the initial radius of the computational domain.

3.1 Passive Stellar evolution: Mass Losses & Heating

The stellar mass-loss rate and the SN Ia are the main ingredients driving the passive stellar evolution. Gas comes mainly from the asymptotic giant branch, red giant and planetary nebula phases (this gas is the fuel which flows down on the central MBH). The gas from the parent stars interacts with the pre-existent ISM and then it heats its kinetic energy to the X-Ray temperature (Mathews 1990, Parriott and Bregman 2008).

According to single burst stellar population synthesis model (Maraston 2005), for solar metallicity and an age $\gtrsim 2\ Gyr$, the rate of stellar mass loss for the whole galaxy is:

$$\dot{M}_\star(t) = 10^{-12} A \cdot M_\star t_{12}^{-1.2} \qquad [M_\odot yr^{-1}] \tag{3.1}$$

where $M_\star$ is the galaxy stellar mass at $t = 12\ Gyr$, t_{12} is time in units of 12 Gyr, and $A = 3.3$ is a coefficient which parametrizes the choice of the IMF function (here the Kroupa IMF, see Pellegrini (2012)). This relation (3.1) is in accord with previous estimates (Mathews 1989, Ciotti, D'Ercole, et al. 1991). Also the SNe Ia enrich the ISM with gas, but above all they warm up the ISM; the input mass due to SNe Ia is given by:

$$\dot{M}_{SN_{Ia}}(t) = 1.4 M_\odot R_{SN_{Ia}}(t) \qquad [M_\odot yr^{-1}] \tag{3.2}$$

where $1.4M_\odot$ is the maximum mass of a stable white dwarf star, above which electron degeneracy pressure in the star's core is insufficient to balance the star's own gravitational self-attraction and then we have the explosion of SN Ia which injects all the mass of the withe dwarfs into the ISM. The term $R_{SN_{Ia}}(t)$ is the rate of SN Ia explosion, which is given by (Greggio 2010)

$$R_{SN_{Ia}}(t) = 0.16 \left(\frac{H_0}{70}\right)^2 10^{-13} L_B t_{12}^{-s} \qquad [yr^{-1}] \tag{3.3}$$

where L_B is the present epoch B-band galaxy luminosity in $L_{B,\odot}$, and s characterizes the secular evolution (recent estimates favour $s \approx 1$, Sharon et al. (2010), Maoz et al. (2011)). Recent observations give $\dot{M}_{SN_{Ia}}(t = 12\ Gyr) = 2.2 \cdot 10^{-13} L_B\ M_\odot yr^{-1}$. Thus, the input mass due to the SNe is ~ 100 times less than the input mass of gas due to the passive stellar evolution given above (3.1), which is:

$$\dot{M}_\star = 2 \cdot 10^{-11} L_B \qquad [M_\odot yr^{-1}]\ . \tag{3.4}$$

Assuming for each supernova event an energy release of $E_{SN_{Ia}} \approx 10^{51}\ erg$, the heating rate provided by SN Ia explosions $L_{SN_{Ia}}(t)$ is given by

$$L_{SN_{Ia}}(t) \approx E_{SN_{Ia}} R_{SN_{Ia}}(t) \qquad [erg\ s^{-1}] \tag{3.5}$$

In Fig. 3.1 we can see from the simulation the quantity of hot mass generated by the stellar evolution, including SNe Ia and retained by a representative model at the end of the run. Some of this gas will be used to form new stars (Fig. 3.2) and accreted on the central MBH.

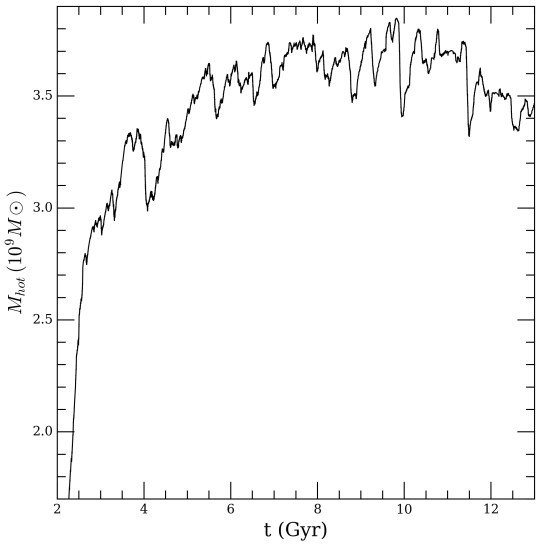

Figure 3.1: Mass of hot gas ($T > 10^6\ K$) within the whole numeric grid.

Also SF and consequent SNII production warm up and enrich of gas the ISM. SF is implemented by subtracting mass, momentum, and energy from the grid; SF also injects new mass and energy from SNII explosions. For each SF episode, assuming that the new stars form with a Salpeter IMF, the mass returned in SNII events is 20% of the new star mass in that episode; the SNII mass source term at each time comes from considering that a given SF episode generates SNe II that inject mass (at a rate exponentially declining on a timescale of $\approx 2 \cdot 10^7\ yr$), and that during the evolution of that episode other episodes may take place, forming other SNIIs that in turn eject mass into the ISM. The same considerations are taken into account to compute the SNII energy injection rate (see Negri et al. (2015) for more details). In Fig. 3.2 we can see the star formation rate and the cumulative mass of new star formed at the end of the run.

The total input mass from stellar evolution is:

$$\dot{M}_{tot}(t) = \dot{M}_{\star}(t) + \dot{M}_{SN_{Ia}}(t) + \dot{M}_{SN_{II}}(t)\ , \tag{3.6}$$

and the total input energy is:

$$L_{tot}(t) = L_{\star}(t) + L_{SN_{Ia}}(t) + L_{SN_{II}}(t)\ , \tag{3.7}$$

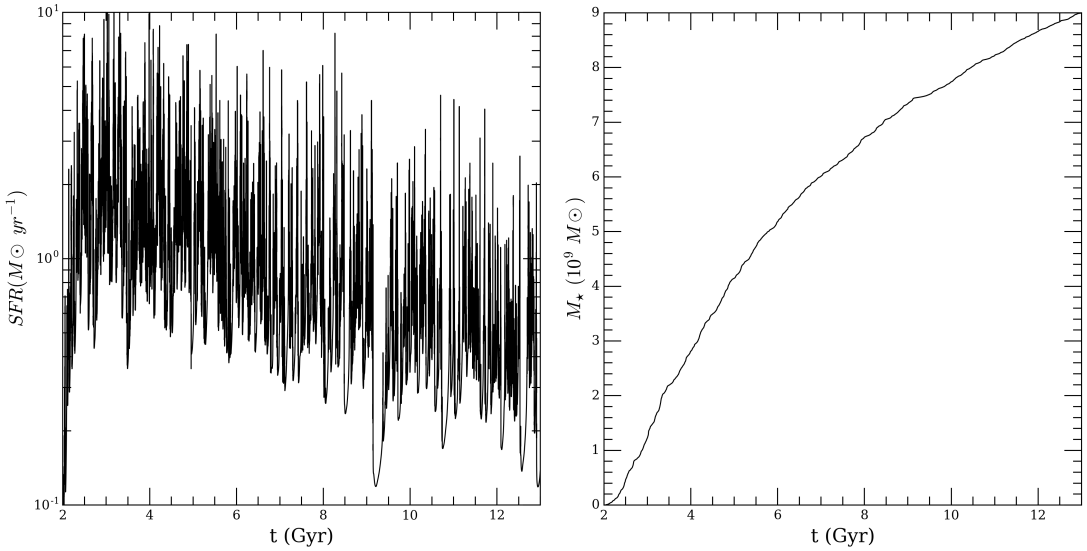

Figure 3.2: From the left to the right panel: SFR in $M_\odot\ yr^{-1}$ and cumulative mass of new star in unit of $10^9 M_\odot$.

where $L_\star$ is the thermalization of the motions of the stars, and it depends on the relative velocity between stars and ISM (for detail see Ciotti, Pellegrini, et al. (2017)).

3.2 Gas Physics

In Sazonov, Ostriker, and Sunyaev (2004), in Ciotti and Ostriker (2007) and in Ciotti, Pellegrini, et al. (2017), the radiative transfer is computed as follows.

The net gas energy rate per unit volume for the gas temperature $T \gtrsim 10^4\ K$ (in cgs system), is defined as:

$$H - C \equiv n^2(S_1 + S_2 + S_3)\ , \tag{3.8}$$

where n is the hydrogen number density; here the positive and the negative terms are grouped respectively together in the two terms of heating (H) and cooling functions (C). The bremsstrahlung losses are given by

$$S_1^{(-)} = -3.8 \cdot 10^{-27}\sqrt{T}\ , \tag{3.9}$$

and the Compton heating and cooling are given by:

$$S_2 = 4.1 \cdot 10^{-35}(T_c - T)\xi\ . \tag{3.10}$$

The sign of S_2 function depends on gas temperature: if $T < T_c$ we have Compton heating, and if $T > T_c$ we have Compton cooling; T_c is the *Compton temperature* (section 3.2.1). S_2 depends also on ξ, that is the *ionization parameter*, which is given by:

$$\xi \equiv \frac{L_{BH}^{eff}(r)}{n(r)r^2} \tag{3.11}$$

where the function $L_{BH}^{eff}(r)$ in 3.11 is the effective accretion luminosity at radius r, which is given by

$$\frac{dL_{BH}^{eff}(r)}{dr} = -4\pi r^2 H(r) \tag{3.12}$$

which, in the case of a spherically symmetric ISM, is integrated radius by radius; along each radius the ISM density and temperature vary as prescribed by the hydrodynamics, so that heating and cooling are not spherically symmetric, but they depend on the 2D ISM properties at each time step of the hydrodynamical simulation. The equation 3.12 is solved with the central boundary condition $L_{BH}^{eff}(r = 0) = L_{BH}$ (as in 2.61 and 2.99).

Finally S_3 describes the photoionization heating, which is given by:

$$S_3^{(+)} = 10^{-23}\frac{b\left(\frac{\xi}{\xi_0}\right)^c}{1 + \left(\frac{\xi}{\xi_0}\right)^c}\frac{Z}{Z_\odot}\ , \tag{3.13}$$

where b is:

$$b = 1.7 \cdot 10^4 T^{-0.7} \tag{3.14}$$

and

$$\xi_0 = \left(\frac{1.5}{T^{0.5}} + \frac{1.5 \cdot 10^{12}}{T^{2.5}}\right)^{-1} + \frac{4 \cdot 10^{10}}{T^2}\left[1 + \frac{80}{e^{(T-10^4)/1.5\cdot 10^3}}\right] . \tag{3.15}$$

The line and recombination continuum cooling:

$$S_3^{(-)} = 10^{-23}\frac{a}{1 + \left(\frac{\xi}{\xi_0}\right)^c}\frac{Z}{Z_\odot} . \tag{3.16}$$

Note that S_3 has an almost-perfect linear dependence on metallicity Z, where:

$$a = -\frac{18}{e^{25(logT-4.35)^2}} - \frac{80}{e^{5.5(logT-5.2)^2}} - \frac{17}{e^{3.6(logT-6.5)^2}} \tag{3.17}$$

and

$$c = 1.1 - \frac{18}{e^{\frac{T}{1.8\cdot 10^5}}} + \frac{4 \cdot 10^1 5}{T^4} . \tag{3.18}$$

The gas temperature is bounded from below by the adopted atomic cooling curve, which has an exponential cut-off below $T \sim 10^4$.
We can write the heating term grouping only the positive terms of 3.8:

$$H \equiv n^2(S_2^{(+)} + S_3^{(+)}) . \tag{3.19}$$

In order to have the idea of how much the ISM absorbs, we can write this heating function in terms of opacity, that we can call *Compton & photoionization absorption coefficient*, κ_{ph}; using the 3.12, we have:

$$\kappa_{ph} = -\frac{1}{\rho(r)L_{BH}^{eff}(r)}\frac{dL_{BH}^{eff}(r)}{dr} = \frac{4\pi r^2 H(r)}{\rho(r)L_{BH}^{eff}(r)} . \tag{3.20}$$

This is a "phenomenological opacity", because it parametrizes the physical absorption phenomena, in which we use the accretion luminosity as a probe of these phenomena.
In the end, the radial forces per unit mass due to radiation that has been absorbed via Compton scattering and photoionization can be written as (see 2.59):

$$\left(\nabla p_{rad}\right)_{ph} = \frac{L_{BH}^{eff}(r)}{4\pi r^3}\frac{\rho(r)\kappa_{ph}}{c}\frac{L_{BH}^{eff}(r)}{4\pi r^2} . \tag{3.21}$$

In Fig. 3.3 we present the temperature and density maps in order to show the complexity of the ISM: we can see that the ISM can have density and temperature fields quite uniform (first and fourth panels from the left), but also a clumped configuration, in which the colder gas is more piled (second and third panels from the left).

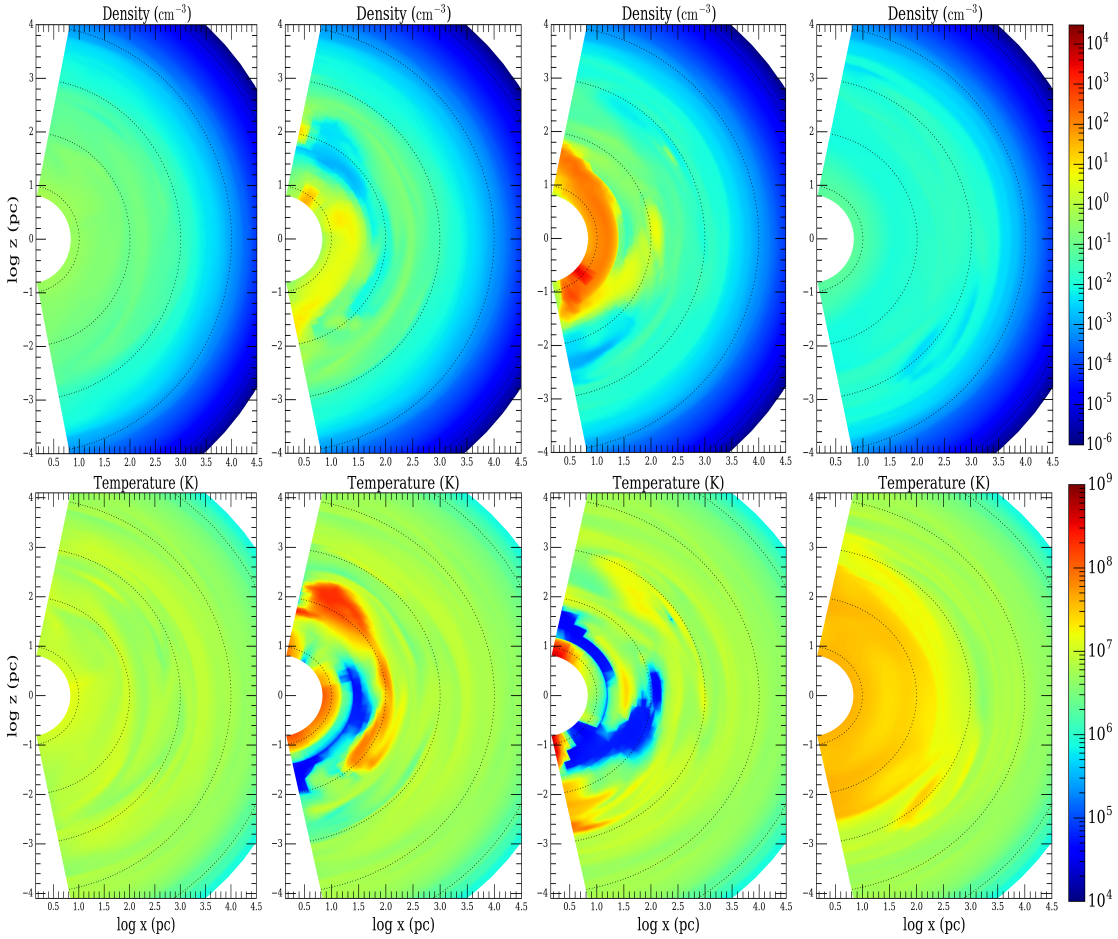

Figure 3.3: Top row: density field in cm^{-3}. Bottom row:temperature field in K. There are four representative times in correspondance with an outburst at 7.45 Gyr with an $L_{BH} \sim 10^{43}\ ergs^{-1}$. From left to right: $t = 7.43\ Gyr$, $t = 7.44\ Gyr$, $t = 7.45\ Gyr$ and $t = 7.46\ Gyr$.

3.2.1 Compton Heating

Compton scattering between electrons and photons is an important and very common process in astrophysics. This type of process can heat the gas (Compton scattering) and it can also cool the gas (inverse Compton scattering). Our interest lies in the impact of radiation on gas, so that we focus only on the heating process.
This process can take place only if the incident photon has an energy $E = h\nu_{ph} \geq m_e c^2$: the difference of these energies is transferred from the photon, which moves to longer wavelengths, to the electron, that acquires momentum, and it heats the gas in which it resides. We can speak in terms of temperature, so dividing the energy of photon and electron with the Boltzmann constant K_B we have two temperature, and the condition become:

$$T_{ph} \geq T_e \tag{3.22}$$

which shows us that there is a characteristic gas temperature above which the incident radiation heats the gas, and this temperature is weighed with the average spectral energy distribution (SED) of the chosen source (in our case, the central MBH), and this one is called *Compton temperature*, T_c. In Sazonov, Ostriker, and Sunyaev (2004) we can find $T_c \simeq 2 \cdot 10^7$ with an accuracy of a factor ~ 2 depending on the type of quasar (obscured vs unobscured); the authors of this article show that the above T_c value is approximately characteristic of both obscured and unobscured quasars.

As we have shown in 3.2, using the 3.10 we can write the opacity which corresponds to the Compton heating, in order to quantify the absorption due to Compton scattering :

$$H_{Comp} = n^2 S_2^{(+)} \ , \tag{3.23}$$

an then using the 3.20 we have

$$\kappa_{Comp} = \frac{4\pi r^2 H_{Comp}(r)}{\rho(r) L_{BH}^{eff}(r)} \ . \tag{3.24}$$

Figure 3.4 shows the maps of Compton opacity from output of hydro simulations of Ciotti, Pellegrini, et al. (2017); we can see how this opacity is quite diffuse, and has always low values. The quantity of absorbed light from the central MBH to the outer region will also depend on the density of the gas (Fig. 3.3); combining the opacity with the gas density we can understand in which optical regime we are. Figure 3.5 shows us the optical depth of Compton opacity, defined as:

$$\tau(r) = \int_{r_0}^{r_1} \rho(r)\kappa(r) dr \ , \qquad r_0 < r_1 \tag{3.25}$$

and we can see that is always $\tau < 1$, so we are in the optically thin regime.

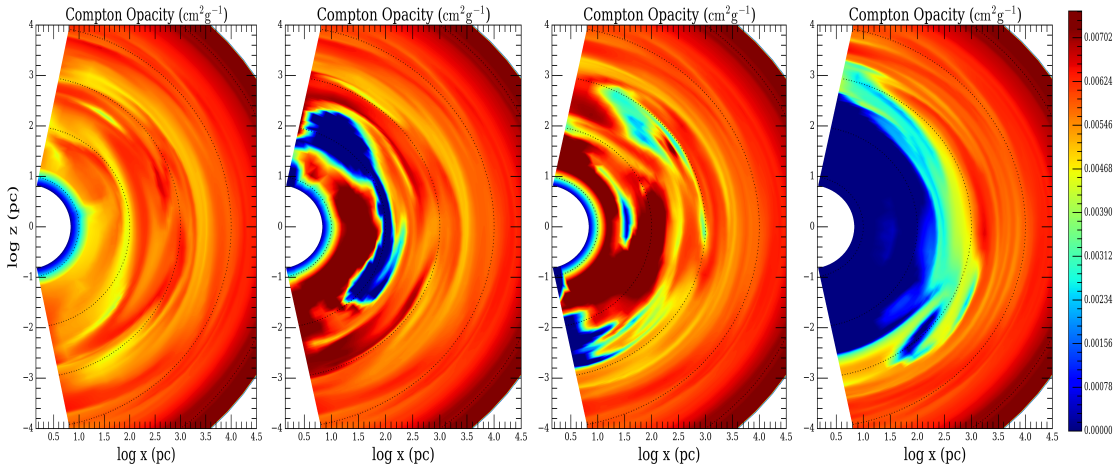

Figure 3.4: Maps of Compton opacity (cm^2g^{-1}) in the representative times of Fig. 3.3.

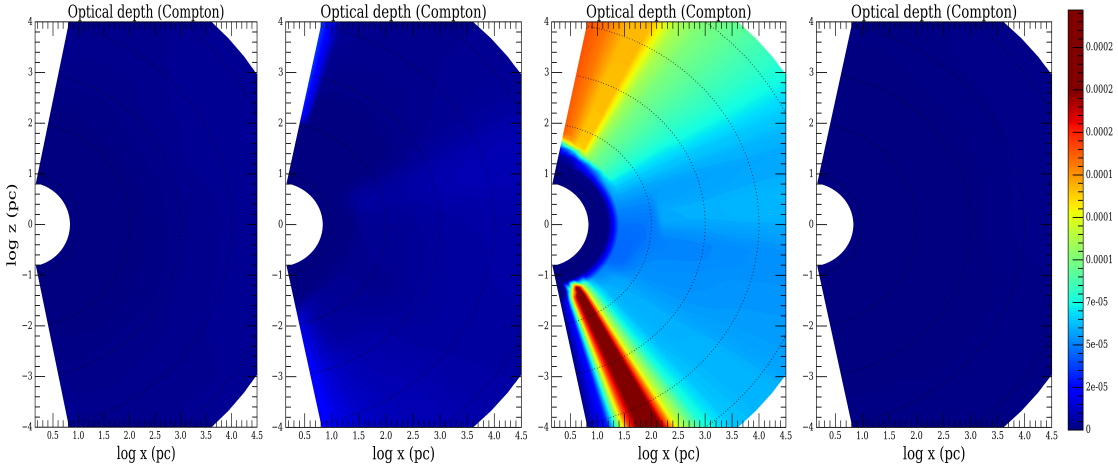

Figure 3.5: Maps of optical depth for Compton opacity in the same representative times of Fig. 3.3. The blue colours shows a trasparent medium.

3.2.2 Partially Ionized Gas Clouds

Another important physical phenomenon which occurs in the ISM is *photoionization*. Gas exposed to intense quasar radiation can be sufficiently dense to remain only partially ionized, and photoionization heating, as well as cooling, through continuum and line emission will then be important. As we have done for the Compton heating, now we introduce κ_{photo}.

We take the $S_3^{(+)}$ function in 3.13 and then we multiply it for the square of number hydrogen density we obtain

$$H_{photo} = n^2 S_3^{(+)} \ . \tag{3.26}$$

Then using the 3.24 we obtain

$$\kappa_{photo} = \frac{4\pi r^2 H_{photo}(r)}{\rho(r) L_{BH}^{eff}(r)} \tag{3.27}$$

As we can see in Fig. 3.6, the photoionization opacity is quite different from the Compton opacity: it is distributed in clouds, and generally can have a value it has greater values than Compton opacity. In order to have a quantitative idea of the absorption, we show in Fig. 3.7 a map of the optical depth due to this opacity.

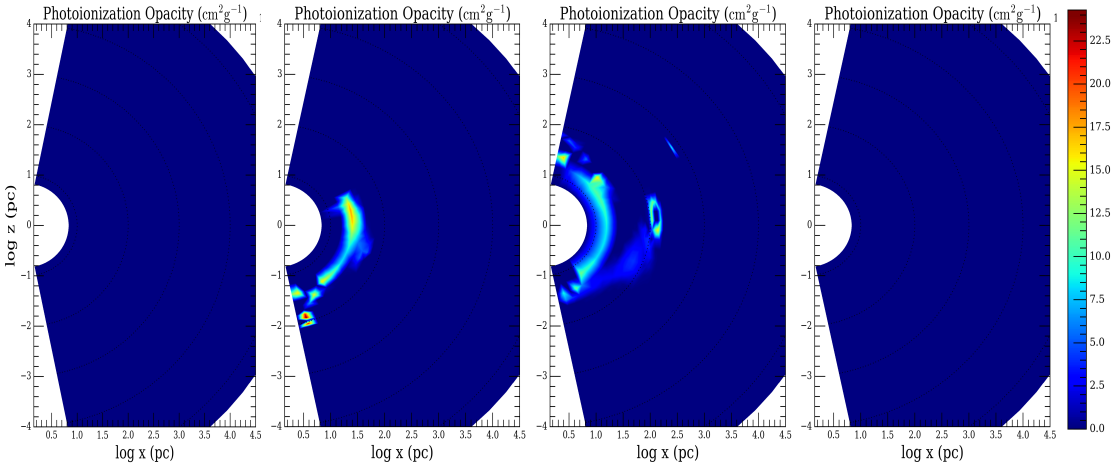

Figure 3.6: Maps of photoionization opacity ($cm^2 g^{-1}$) in the representative times of Fig. 3.3

We can see that we are always in a optically thin regime, but we often get close to the

optically thin regime limit (in some cases τ approaches and can exceed 1). Moreover, this type of absorption is strongly dependent on the angular distribution of the cold material.

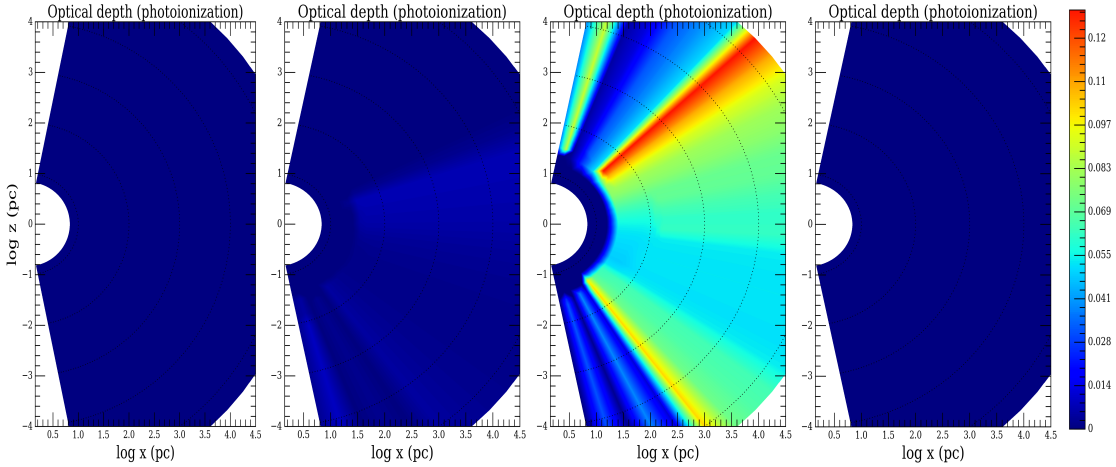

Figure 3.7: Maps of optical depth for photoionization opacity in the same representative times of Fig. Fig. 3.3.

3.2.3 Electron Scattering

Let us consider the simplest radiative transfer problem in which such a ray coupling plays a role. Suppose we have a medium consisting of small particles that can scatter radiation in arbitrary directions. This process is called *isotropic scattering*, because the outgoing direction of a photon has, by assumption, no dependence on the direction of the photon before the scattering event. Let us also assume that the particles do not absorb nor emit any of the radiation, and let us focus on a single frequency ν. Let us also assume that somewhere (either inside or outside of the scattering cloud) there is a source of light, which we will treat as an initial value for the intensity at the start of rays emanating from that source (Fig. 3.8).

This is the case of *electron scattering*: we assume that all the radiation, in the whole

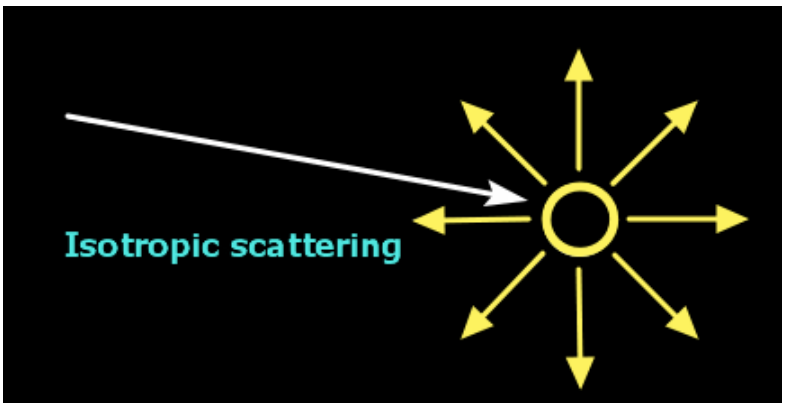

Figure 3.8: Isotropic scattering.

spectrum, will be scattered by the medium, proportionally to the intensity of the radiation field and also to the medium density:

$$\tau_{es} = \int_{s}^{s+ds} \rho(s')\kappa_{es} ds' \tag{3.28}$$

where ρ is the gas density, κ_{es} does not depend on position, therefore is constant $\kappa_{es} = 0.35$ (Ciotti, Pellegrini, et al. 2017) and ds is the optical path of radiation.

We stress that the presence of electron scattering does not have an impact on variation of radiation field in the D Model (equation 2.136), but it has a role just in the radiation pressure (equation 2.81); on the contrary, the electron scattering plays a fundamental role in the AD Model (equation 2.137).

3.3 Dust Physics

Giant elliptical galaxies generally have an optically thin ISM, with a negligible presence of interstellar dust. Observations indicate to us that Quasars emit near (or equal) to their *Eddington limit*, which is calculated using the scattering Thomson opacity $\kappa_{es} = 0.35\ cm^2 g^{-1}$; in comparison with the typical opacity of dust grains in different electromagnetic bands (Ciotti and Ostriker 2007; Novak et al. 2012; Hensley et al. 2014) we have that Thomson opacity is $\sim 10^3$ times smaller than dust opacity (Tab 3.3).

Band	Energy	Fraction	Dust Opacity
X-ray	E $>$ 2 keV	0.7	
UV	13 eV $<$ E $<$ 2 keV	0.2	3920 κ_{es}
Optical	1 eV $<$ E $<$ 13 eV	0.1	979 κ_{es}

Table 3.1: Table of dust opacity in the three band (UV, OPT and IR)for solar metallicity gas with Milky Way dust-to-gas ratio expressed in terms of the electron scattering opacity $\kappa_{es} = 0.35\ cm^2 g^{-1}$, assumed unabsorbed AGN energy output by band (Sazonov, Ostriker, and Sunyaev 2004).

Because of this difference between the opacities, radial forces on dust grains due to radiation from the AGN can easily overpower the other dynamic drivers during AGN flaring.
The existence of obscured and unobscured quasars, added to the observational fact that in elliptical galaxies in a "off phase" of AGN there is not dust, indicates us that dust in these type of objects has a parallel dynamical evolution with the AGN phase "on" and "off". Hensley and collaborators (Hensley et al. 2014) have found that during the cooling flow phases the radiative pressure on dust grains in the cold gas shells infalling onto the central MBH can greatly impact on the gas available for accretion, and consequently on the frequence and the time-scale of outburst.

We must of course take into account the fact that dust can absorb radiation very efficiently in the UV and Optical bands, and it reprocesses and re-emits this light in the IR band, and this can have a great impact on the gas dynamics. Indeed, obscured AGN IR Spectral Energy Distribution (SED) is dominated by thermal emission from dust (Neugebauer et al. 1979), heated by the primary Optical and UV continuum (dominating the unobscured AGN SEDs). According to observations, in Hensley et al. (2014) it was estimated that the re-emission of the IR radiation due to warm dust can dominate the bolometric luminosity of galaxy during the early phases of AGN bursts, which can reach $\sim 10^{46}\ erg\ s^{-1}$.

In addition, infalling shells of cold gas can be supported by radiative pressure and slowing down the accretion can have an impact on the gas quantity available for residual star formation (the so called "positive feedback", Ciotti, Ostriker, Novak, et al. 2015) at late times.

In this work we chose to treat dust opacity as in Ciotti and Ostriker (2007), with the

confirmation of this view by Hensley et al. (2014), in which the dust opacity (in cm^2g^{-1}) is divided in three broad bands: UV, Optical and IR, while:

$$\kappa_{opt} = \frac{300}{1 + T/10^4} \qquad \kappa_{UV} = 4\kappa_{opt} \qquad \kappa_{IR} = \frac{\kappa_{opt}}{150} \ . \tag{3.29}$$

We have also divided the bolometric accretion luminosity in broad bands (as in 3.3):

$$L_{BH,X} = 0.7L_{BH}, \qquad L_{BH,opt} = 0.1L_{BH}, \qquad L_{BH,UV} = 0.2L_{BH} \tag{3.30}$$

while the infrared luminosity is produced by the reprocessing of absorbed radiation from dust:

$$L_{BH,IR} = L^{abs}_{BH,UV} + L^{abs}_{BH,Opt} \ . \tag{3.31}$$

In this work we have not computed the reprocessed light, but we plan to do the same study adding this IR light and the relative pressure on dust grains. The $L_{BH,X}$ heat the gas via processes explained in section 3.2.

As we can see from the 3.29, the temperature dependent denominator is designed to mimic the destruction of dust (sputtering) at high temperatures; also, these opacities have the same spatial distribution, but they are different in absolute values.

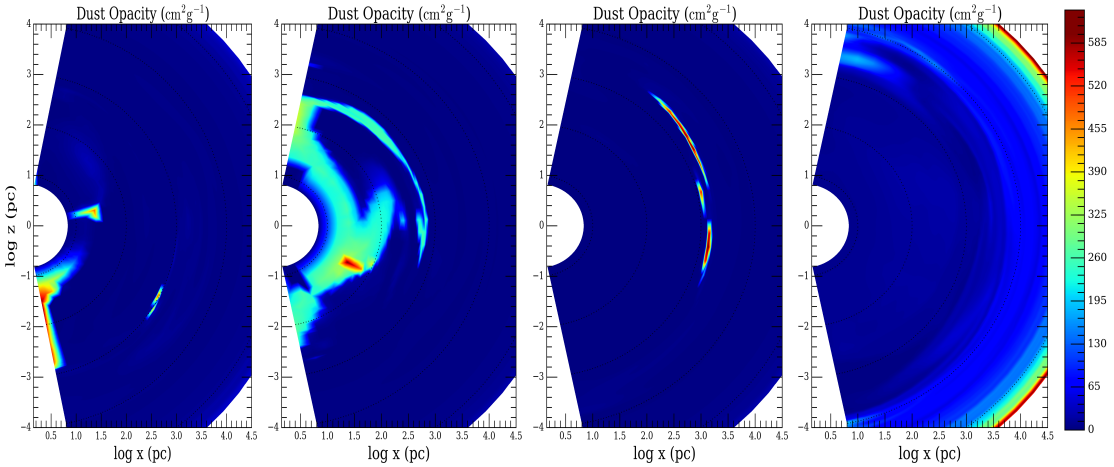

Figure 3.9: Maps of dust opacity (cm^2g^{-1}). There are four representative times in correspondance with an outburst at 7.11 Gyr with an $L_{BH} \sim 3 \cdot 10^{43}\ ergs^{-1}$. From left to right: $t = 7.10\ Gyr$, $t = 7.11\ Gyr$, $t = 7.12\ Gyr$ and $t = 7.13\ Gyr$.

Furthermore, we can see that τ can exceed 1 very easily; thus shows the importance to

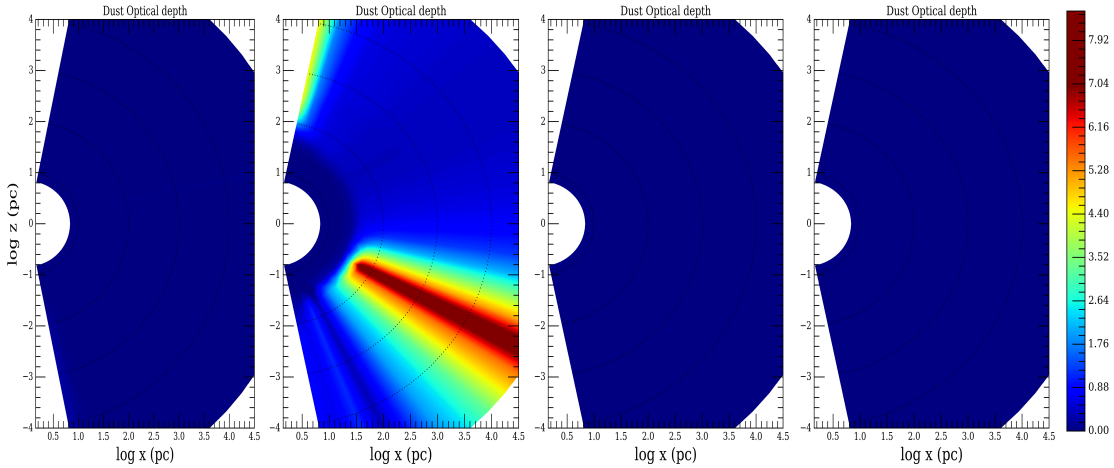

Figure 3.10: Maps of optical depth for dust in the representative times of Fig. 3.9.

find a new model of radiative transfer which can interpolate the optically thin regime and also the optically thick regime (the presence of dust is crucial). The optical depth for dust is computed as follow:

$$\tau_{dust} = \int_{s}^{s+ds} \rho(s')(\kappa_{uv}(s') + \kappa_{opt}(s') + k_{es})ds' \tag{3.32}$$

with the same definitions of the 3.28.
Finally, the radiative pressure gradient is computed using the unabsorbed light separately for each bands, using the relative opacity and equation 2.80.